Existence and numerical stability study of weak solutions of a Maxwell fluid in a channel. (English version of "Existence et étude numérique de stabilité de solutions faibles du problème de fluide de Maxwell dans un canal"). Publication de l'Institut Camille Jordan n° 413, 29 p. (2022). English Version

Dominique Sandri

D. Sandri

Université de Lyon 1, Institut Camille Jordan (UMR 5208), Bât. Jean Braconnier, 21 Avenue Claude Bernard, 69622 VILLEURBANNE CEDEX, FRANCE.

Existence and numerical stability study of weak solutions of a Maxwell fluid in a channel.

Abstract. We study the flow of a fluid governed by the corotational Maxwell model (COM model) or the upper convected Maxwell model (UCM model) through a plane channel. It appears that the problem admits a weak solution, in a sense to be specified, which is a flow exhibiting slip at the walls of the channel. This kind of solution presents stability properties that could explain the slip phenomenon observed in the simulations performed in [13], [14], [15] and give indications on the problem of the High Weissenberg Number (see [8]).

1. Introduction. When we consider the flow of a fluid governed by the upper convected Maxwell model (important case of modeling of polymer without solvent) through an abrupt contraction and that the solution of this problem is approached by a finite element method (FEM), the methods used to solve the non-linear FE problem start to diverge with mesh refinement (High Weissenberg number problem).

The method introduced in [2] so called the log-conformation method, allows to remedy analogous situations and allows to reach large Weissenberg numbers in the simulations. However, as noticed in the case of a simulation of 3D flow in an abrupt contraction for a fluid governed by the Oldroyd model, no significant improvements appear, with this method, in the case of the upper convected Maxwell problem (see [1]).

On the other hand, as noted in [16], in the case of a non zero Reynolds number ($Re = 1$), the author observes an unresolved structure in the solution downstream from the reentrant corner *that may or may not be a numerical artifact*. The study shows that a very high level of resolution close to the geometric singularity (at the reentrant corner of the contraction) would be necessary to approach this singularity.

In [12], we have developed a method (to simplify our purpose, we will name this method θ-MSUPG method) which would seem to be the only one, to our knowledge, that allows us to obtain convergence results of the FEM for the approximation of a linearized version of Maxwell's problem, the linearization intervening on the velocity terms in the constitutive equation. The simulations with this method then show a slip at the downstream wall of the flow in a 4 :1 contraction, for the models COM and UCM (*cf.* [13]).

Knowing that this phenomenon can be an artifact of simulation, we study in this article, this issue of wall slip in the case of a flow in a plane channel. In the case of a flow in a channel of infinite length of a fluid governed by the Maxwell model (COM and UCM), we show the existence of weak solutions with slip at the wall for this type of of flow. Then, we study the stability of these weak solutions. For this, we consider the case of a flow through a finite channel, with boundary conditions, and we approach the problem thus posed, by a finite element method. We look at the extent to which the approximate flow stabilizes downstream of the flow towards the restriction to the finite domain of a weak solution obtained on the infinite domain. For sufficiently large Weissenberg numbers, we observe that the flow given by the approximated solution stabilizes around a weak solution. In particular, with the θ-MSUPG method, if the boundary conditions are given by the values of a weak solution, we observe a convergence of the finite element solutions to this weak solution, for sufficiently large Weissenberg numbers. This leads us to make the hypothesis that this type of weak solution would exist in the case of a 4 :1 contraction, without excluding the possible existence of a strong joint solution, with

a corner singularity (*cf.* the study in [7]). The phenomenon of the high Weissenberg number problem for the Maxwell model with upper convection would then occur with mesh refinement which would make weak solutions more attractive but of unstable numerical approximation for methods of type SUPG. The θ-MSUPG method would allow a better approximation of these solutions.

In Section 2, we consider the problem of one-dimensional flow in a channel of infinite length with a condition of zero velocity at the wall of a fluid governed by the the viscoelastic corotational Maxwell model (COM) or the upper convected Maxwell model (UCM). We build weak solutions, in a sense to be defined, of this problem. In Section 3, we will consider a flow in a channel of finite length, with boundary conditions. The resulting problem is approached by various FE methods, with a fixed point method to solve the nonlinear problem. We then study the stabilization of the approximate solutions towards the weak solutions obtained at §2, on the whole flow, or on a part of it.

2. Existence of weak solution for a Poiseuille flow. Let denote σ the extra-stress-tensor, u the fluid velocity and p its pressure. We assume that the extra-stress tensor σ is symmetric. We have denoted $\nabla.\sigma = \sigma_{ij,j}$ the divergence of the tensor σ, with the Einstein summation convention, $\sigma : \tau$ the sum $\sigma_{ij}\tau_{ij}$, $\nabla.u = u_{i,i}$ the divergence of u, $u.\nabla\sigma = u_k\sigma_{ij,k}$, $\nabla p = p_{,i}$ the gradient of p, $d(u) = \frac{1}{2}(u_{i,j} + u_{j,i})$ the rate of strain tensor of u and $\omega(u) = \frac{1}{2}(u_{i,j} - u_{j,i})$ the vorticity tensor of u.

Let $a \in [-1, 1]$, we set B be the objective derivative

$$B(u, \sigma) = u.\nabla\sigma + \sigma\omega(u) - \omega(u)\sigma - a(d(u)\sigma + \sigma d(u)).$$

We consider the flow of a fluid through the domain $\Omega =]-\infty, +\infty[\times]-1, 1[$ with boundary $\Gamma =]-\infty, +\infty[\times\{-1, 1\}$, with (σ, u, p) satisfying the Oldroyd model :

$$(\mathcal{P}) \begin{cases} \sigma + \lambda B(u, \sigma) = 2\alpha d(u) \text{ in } \Omega, \\ -\nabla.\sigma - 2(1-\alpha)\nabla.d(u) + \nabla p = 0 \text{ in } \Omega, \\ \nabla.u = 0 \text{ in } \Omega, \\ u(x, -1) = u(x, 1) = 0, \forall x \in \mathbb{R}\,, \end{cases}$$

where $0 \leq \alpha \leq 1$ is the viscoelastic fraction of the viscosity. The Maxwell model, which we will consider in the following, is obtained setting $\alpha = 1$ in $(\mathcal{P})$. For $\alpha = 1$ and $a = 0$, the problem $(\mathcal{P})$ is the corotational Maxwell model (COM Model), and for $\alpha = 1$ and $a = 1$, this problem is the upper convected Maxwell model (UCM model).

We are looking for a one-dimensional flow solution of $(\mathcal{P})$, with u and σ depending only on the variable y and such that $u_2 = 0$, which we will call Poiseuille flow.

Let $\alpha = 1$, we will say that (σ, u, p) is a weak solution of $(\mathcal{P})$, if (σ, u, p) is the pointwise limit on Ω, when ϵ tends to 0^+, of a sequence of one-dimensional flows $(\sigma^\epsilon, u^\epsilon, p^\epsilon)$ such that for all bounded open set of the kind $\Omega_\ell =]-\ell, \ell[\times]-1, 1[$, $\ell > 0$, we have $(\sigma^\epsilon, u^\epsilon, p^\epsilon) \in [L^2(\Omega_\ell)]^4 \times [H^1(\Omega_\ell)]^2 \times L^2(\Omega_\ell)$, $u^\epsilon.\nabla\sigma^\epsilon \in [L^2(\Omega_\ell)]^4$ and

$$(\mathcal{P}f) \begin{cases} \lim_{\epsilon\to 0^+} \sigma^\epsilon + \lambda B(u^\epsilon, \sigma^\epsilon) - 2d(u^\epsilon) = 0 \text{ in } [L^1_{loc}(\Omega)]^4, \\ \lim_{\epsilon\to 0^+} -\nabla.\sigma^\epsilon + \nabla p^\epsilon = 0 \text{ in } [H^{-1}(\Omega)]^2, \\ \nabla.u^\epsilon = 0 \text{ in } \Omega, \\ u^\epsilon(x, -1) = u^\epsilon(x, 1) = 0, \forall x \in \mathbb{R}\,. \end{cases}$$

We then have the following result (the pressures are defined up to an additive constant C_p) :

Proposition 1. Let $\alpha = 1$ and let $D > 0$ (where D represents the flow rate).

• *Case 1. Let $a = 0$ (Corotational Maxwell Model).*

a) If $\lambda \leq \lambda_c \overset{\text{déf}}{=} \frac{2}{D}(1 - \frac{\pi}{4})$, then there exists a unique Poiseuille flow of class $\mathcal{C}^1(\Omega)$ solution of Problem $(\mathcal{P})$, such as (u, p) satisfies :

$$(1)\ u_1(x,y) = \int_1^y \frac{-2fs}{1+\sqrt{1-4f^2\lambda^2 s^2}}\,ds,\ u_2(x,y) = 0, p(x,y) = -fx + C_p, \int_{-1}^{1} u_1(x,y)dy = D.$$

The constant $0 \leq f \leq f_\lambda \overset{\text{déf}}{=} \frac{1}{2\lambda}$ is uniquely defined by the flow rate condition.

b) For $\lambda > \lambda_c$, there is no Poiseuille flow of class $\mathcal{C}^1(\Omega)$ solution of $(\mathcal{P})$.

c) Problem $(\mathcal{P})$ admits a weak solution given by

$$\begin{aligned} &\sigma = 0, u = (U_0, 0), p = C_p \text{ in } \Omega \text{ and} \\ &\sigma = \begin{pmatrix} \frac{1}{\lambda} & 0 \\ 0 & -\frac{1}{\lambda} \end{pmatrix}, u = (0,0), p = -\frac{1}{\lambda} + C_p \text{ on } \Gamma,\ U_0 = \frac{D}{2}. \end{aligned} \tag{2}$$

• *Case 2. Let $a = 1$ (Upper convected Maxwell Model).*

a) For all $D \geq 0$, there exists a unique Poiseuille flow of class $\mathcal{C}^1(\Omega)$ solution of $(\mathcal{P})$, such that (u, p) satisfies :

$$u_1(x,y) = \frac{f}{2}(1-y^2),\ u_2(x,y) = 0, p(x,y) = -fx + C_p, f = \frac{3}{2}D. \tag{3}$$

b) Problem $(\mathcal{P})$ admits a weak solution, with σ_{11} defined up to an additive constant C_σ on Γ, given by

$$\begin{aligned} &\sigma = 0, u = (U_0, 0), p = C_p \text{ in } \Omega \text{ and} \\ &\sigma = \begin{pmatrix} C_\sigma & 0 \\ 0 & -\frac{1}{\lambda} \end{pmatrix}, u = (0,0), p = -\frac{1}{\lambda} + C_p \text{ on } \Gamma,\ U_0 = \frac{D}{2}. \end{aligned} \tag{4}$$

Proof. For convenience, we resume the proof of the relation (1) given in [6], which we complete with the question of the flow rate. We have kept the variable x in the expressions of (σ, u) and we have kept the writing of the partial derivatives.

Proof of case 1 (COM model), $a) - b)$. For $a = 0$, with $u.\nabla\sigma = 0$, the constitutive equation can be written as :

$$\sigma_{11} - \lambda\sigma_{12}u_{1,2} = 0, \sigma_{12} + \frac{\lambda}{2}(\sigma_{11} - \sigma_{22})u_{1,2} - u_{1,2} = 0, \sigma_{22} + \lambda\sigma_{12}u_{1,2} = 0,$$

this gives the classic relation

$$(5)\ \sigma_{11}(x,y) = \frac{\lambda u_{1,2}^2(x,y)}{1+\lambda^2 u_{1,2}^2(x,y)}, \sigma_{12}(x,y) = \frac{u_{1,2}(x,y)}{1+\lambda^2 u_{1,2}^2(x,y)}, \sigma_{22}(x,y) = -\frac{\lambda u_{1,2}^2(x,y)}{1+\lambda^2 u_{1,2}^2(x,y)},$$

$$u_{1,2} = \frac{1 \pm \sqrt{1-4\lambda^2\sigma_{12}^2}}{2\lambda^2\sigma_{12}} = \frac{2\sigma_{12}}{1 \mp \sqrt{1-4\lambda^2\sigma_{12}^2}} \text{ if } \sigma_{12} \neq 0 \text{ and } 1 - 4\lambda^2\sigma_{12}^2 \geq 0,$$

$$u_{1,2} = 0 \text{ if } \sigma_{12} = 0.$$

The momentum equation can be written as :

$$-\sigma_{12,2} + p_{,1} = 0, -\sigma_{22,2} + p_{,2} = 0,$$

we obtain a pressure of the form

$$p(x,y) = \sigma_{22}(x,y) + \Psi(x) \Rightarrow \sigma_{12,2}(x,y) = \Psi'(x) \Rightarrow \sigma_{12}(x,y) = \Psi'(x)y + K(x).$$

Since σ_{12} depends only on y, we deduce that Ψ' is a constant denoted by $-f$ and that the function K is constant. We then have $p_{,1} = -f$. With (5), we then obtain :

$$\sigma_{12} = -fy + K \Leftrightarrow u_{1,2} = (-fy + K)(1 + \lambda^2 u_{1,2}^2).$$

By assumption, u does not depend on x and must verify the boundary conditions $u_1(x,-1) = u_1(x,1) = 0$, therefore, according to the mean value theorem, $u_{1,2}$ vanishes for a value $-1 < y_0 < 1$ and therefore $K = fy_0$. This gives with (5) :

$$u_{1,2}(x,y) = \frac{-2f(y-y_0)}{1 \pm \sqrt{1 - 4\lambda^2 f^2 (y-y_0)^2}} \text{ if } 1 - 4\lambda^2 f^2 (y-y_0)^2 \geq 0 \text{ and } y \neq y_0.$$

We obtain the only possible continuous function defined in the neighbourhood of y_0 :

$$u_{1,2}(x,y) = \frac{-2f(y-y_0)}{1 + \sqrt{1 - 4\lambda^2 f^2 (y-y_0)^2}}$$

which is defined on $[-1,1]$ for λ sufficiently small. It remains to satisfy the boundary conditions. So we have

$$u_1(x,y) = \int_1^y \frac{-2f(s-y_0)}{1 + \sqrt{1 - 4\lambda^2 f^2 (s-y_0)^2}}\, ds = \int_{1-y_0}^{y-y_0} \frac{-2fs}{1 + \sqrt{1 - 4\lambda^2 f^2 s^2}}\, ds.$$

The function to be integrated is odd and has the sign of $-f$ strictly for $s > 0$. The boundary condition $u_{1,2}(x,-1) = 0$ is satisfied if and only if $-1 - y_0 = -(1 - y_0) \Rightarrow y_0 = 0$. Then, if $|f| \leq f_\lambda$, with $f_\lambda = \frac{1}{2\lambda}$, we obtain a unique Poiseuille flow of class $\mathcal{C}^1(\Omega)$ solution of $(\mathcal{P})$ defined up to the constant f, with u given by

$$u_1(x,y) = \int_y^1 \frac{2fs}{1 + \sqrt{1 - 4f^2\lambda^2 s^2}}\, ds,\ u_2(x,y) = 0. \tag{6}$$

For this result, one can refer, for example, to [6], Eqn. 2.8 and Proposition 2.1 (for a flow in the direction of y).

It remains to show the existence of the solution for a given flow rate D. Let u_1 be given by (6) and let $D(f) = \int_{-1}^1 u_1(x,y)dy = 2\int_0^1 u_1(x,y)dy$ the flow rate. For $\lambda \in \mathbb{R}$ and $s \in]0,1]$ given, the function of the variable f : $f \to \frac{2fs}{1+\sqrt{1-4f^2\lambda^2 s^2}}$ is continuous, strictly increasing as product of strictly increasing positive functions. From this we can deduce that for $y \in [-1,1]$ to be given, $u_1(x,y)$ is a strictly increasing function of f and that D is a strictly increasing continuous bijection of $[0, f_\lambda]$ to $[0, D(f_c)]$. The maximum flow rate is reached for $f = f_\lambda$ and its value is

$$D(f_\lambda) = \frac{2}{\lambda}\int_0^1 (\int_y^1 \frac{x}{1 + \sqrt{1-x^2}} dx)dy = \frac{1}{\lambda}(1 - \frac{\pi}{4}).$$

Thus a given flow rate $D \geq 0$ can be satisfied by the fluid if and only if λ satisfies :

$$D \leq \frac{2}{\lambda}(1-\frac{\pi}{4}) \Leftrightarrow \lambda \leq \lambda_c \overset{\text{déf}}{=} \frac{2}{D}(1-\frac{\pi}{4}). \ \square$$

In the case $\lambda \leq \lambda_c$, the constant f is uniquely determined. Thus for $\lambda > \lambda_c$, there is no more existence of a Poiseuille flow of class $\mathcal{C}^1(\Omega)$. In the numerical simulations in a channel Ω_L presented in the next Section, it appears that the flow generally stabilizes towards the regular Poiseuille flow (1), when there exists a solution given by (6) which satisfies the imposed flow rate D in the simulation, *i.e.* for $\lambda \leq \lambda_c$ (see also [14], [15], Fig. 3.2). A flow with wall slip appears when λ becomes larger than λ_c, *i.e.* when we lose the existence of the Poiseuille flow and a pressure drop appears. The flow with a wall slip then stabilizes around the weak solution (2).

Proof of case 1 (COM model), *c*) **Existence of the weak solution.** Let $0 < \epsilon < 1$. We set f_ϵ and $g_\epsilon = 1 - f_\epsilon$, the respective indicator functions of $\Omega^\epsilon =]-\infty, +\infty[\times[-1+\epsilon, 1-\epsilon]$ and its complement in $\bar{\Omega} = \Omega \cup \Gamma$: $(\Omega^\epsilon)^c =]-\infty, +\infty[\times[-1, -1+\epsilon[\cup]-\infty, +\infty[\times]1-\epsilon, 1]$. Then, for $(x, y) \in \bar{\Omega}$, we have :

$$f_\epsilon(x,y) = 1 \ \textit{if} \ -1+\epsilon \leq y \leq 1-\epsilon, f_\epsilon(x,y) = 0, \textit{otherwise},$$
$$g_\epsilon(x,y) = 0 \ \textit{if} \ -1+\epsilon \leq y \leq 1-\epsilon, g_\epsilon(x,y) = 1, \textit{otherwise}.$$

We set $U_0 = 2D$, with $D > 0$ the flow rate, we set u_1^ϵ be the continuous function with value U_0 on Ω^ϵ, $\frac{(1+y)U_0}{\epsilon}$ on $]-\infty, +\infty[\times[-1, -1+\epsilon[$ and $\frac{(1-y)U_0}{\epsilon}$ on $]-\infty, +\infty[\times]1-\epsilon, 1]$ (see Fig. 1) and we set u_2^ϵ be the zero function on $\bar{\Omega}$.

The function u_1^ϵ is a piecewise $\mathcal{C}^1$ function which belongs to $H^1(\Omega_\ell), \forall \ell > 0$. The directional derivative of u_1^ϵ along the direction x is null. We have

$$u^\epsilon(x,y) = U_0(f_\epsilon + \frac{1-|y|}{\epsilon} g_\epsilon, 0).$$

The velocity profile of u^ϵ has then the shape of a trapezoid (see Fig. 1). The function u_1^ϵ has partial derivative with respect to y on the set $\bar{\Omega}$ minus the lines $y = -1+\epsilon$ and $y = 1-\epsilon$, with

$$u_{1,2}^\epsilon(x,y) = -sign(y)\frac{U_0}{\epsilon} g_\epsilon, y \neq -1+\epsilon, y \neq 1-\epsilon.$$

We set, from (5) :

$$\sigma_{11}^\epsilon = \frac{\lambda U_0^2}{\epsilon^2 + \lambda^2 U_0^2} g_\epsilon, \sigma_{12}^\epsilon = -sign(y)\frac{\epsilon U_0}{\epsilon^2 + \lambda^2 U_0^2} g_\epsilon, \sigma_{22}^\epsilon = -\frac{\lambda U_0^2}{\epsilon^2 + \lambda^2 U_0^2} g_\epsilon, p^\epsilon = \sigma_{22}^\epsilon + C_p.$$

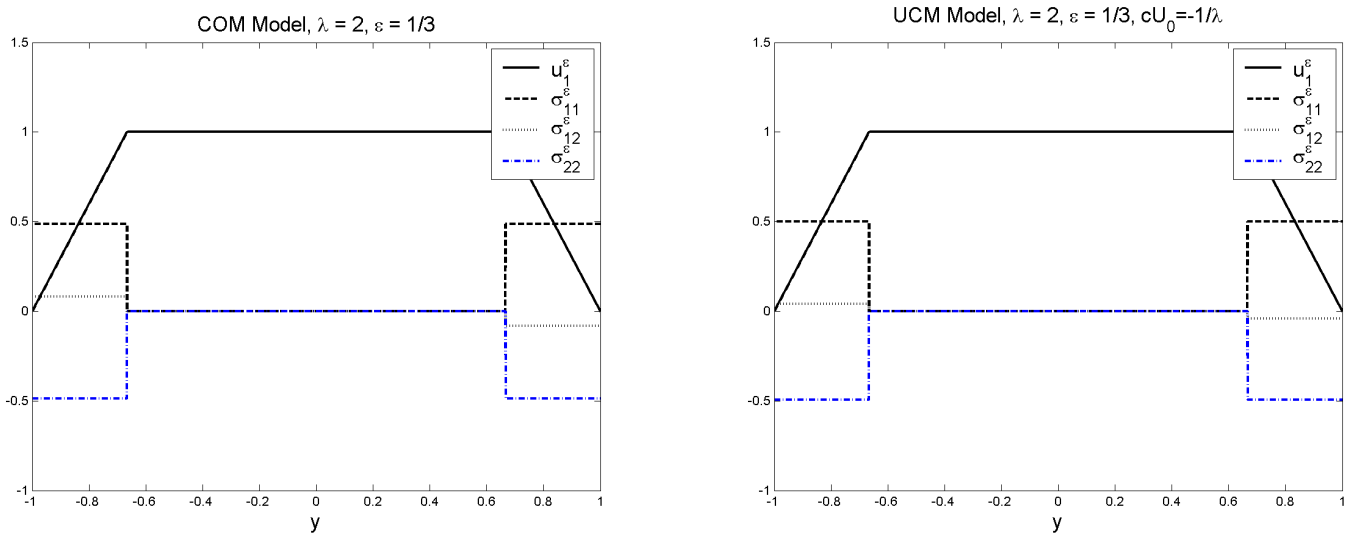

Fig. 1. Functions σ^ϵ and u_1^ϵ in the case of the COM model and in the case of the UCM model, with $U_0 = 1$ and, in the case of the UCM model, $c = \frac{1}{\lambda}$.

The tensor σ^ϵ admits a directional derivative along the vector u^ϵ with zero value : $u^\epsilon.\nabla\sigma^\epsilon = u_1^\epsilon\sigma_{,1}^\epsilon = 0$. Let (σ, u, p) be the pointwise limit function of $(u^\epsilon, \sigma^\epsilon, p^\epsilon)$ when ϵ tends to 0^+ on the closed set $\bar{\Omega} = \Omega \cup \Gamma$, the triple (σ, u, p) satisfies the Eqn. (2) of Proposition 1 :

$$u = (U_0, 0), \sigma = 0, p = 0 \text{ in } \Omega \text{ and } u = (0,0), \sigma = \begin{pmatrix} \frac{1}{\lambda} & 0 \\ 0 & -\frac{1}{\lambda} \end{pmatrix}, p = -\frac{1}{\lambda} + C_p, \text{ on } \Gamma.$$

The triple (σ, u, p) is a constant function on Ω and then it satisfies the Problem $(\mathcal{P})$, but with a discontinuous velocity at the boundary. The triple $(\sigma^\epsilon, u^\epsilon, p^\epsilon)$ satisfies the constitutive equation for $y \neq \pm(1-\epsilon)$:

$$\sigma^\epsilon + \lambda B(u^\epsilon, \sigma^\epsilon) - 2d(u^\epsilon)$$
$$= \begin{pmatrix} \sigma_{11}^\epsilon - \lambda\sigma_{12}^\epsilon u_{1,2}^\epsilon & \sigma_{12}^\epsilon + \frac{\lambda}{2}(\sigma_{11}^\epsilon - \sigma_{22}^\epsilon)u_{1,2}^\epsilon - u_{1,2}^\epsilon \\ \sigma_{12}^\epsilon + \frac{\lambda}{2}(\sigma_{11}^\epsilon - \sigma_{22}^\epsilon)u_{1,2}^\epsilon - u_{1,2}^\epsilon & \sigma_{22}^\epsilon + \lambda\sigma_{12}^\epsilon u_{1,2}^\epsilon \end{pmatrix} = \begin{pmatrix} 0 & 0 \\ 0 & 0 \end{pmatrix}$$

and then

$$\lim_{\epsilon \to 0^+} \sigma^\epsilon + \lambda B(u^\epsilon, \sigma^\epsilon) - 2d(u^\epsilon) = 0 \text{ in } [L^1_{loc}(\Omega)]^4.$$

The choice of the $L^1_{loc}(\Omega)$ convergence is due to the fact that $B(u^\epsilon, \sigma^\epsilon) \in L^1_{loc}(\Omega)$ when $(\sigma^\epsilon, u^\epsilon)$ belongs in $[L_2(\Omega_\ell)]^4 \times [H^1(\Omega_\ell)]^2$ for all $\ell > 0$.

We denote by $\langle\,,\rangle$ the duality bracket for the dual pair $([\mathcal{D}(\Omega)]^2)'$ and $[\mathcal{D}(\Omega)]^2$. Let $v \in [\mathcal{D}(\Omega)]^2$, let K be the compact support of v and let ϵ_0 such that $K \subset \Omega^\epsilon, \forall 0 < \epsilon \leq \epsilon_0$, then, since σ^ϵ and p^ϵ are zero on K, for $0 < \epsilon < \epsilon_0$ we have :

$$\langle -\nabla.\sigma^\epsilon + \nabla p^\epsilon, v\rangle = (\sigma^\epsilon, d(v)) - (p^\epsilon, \nabla.v) = \int_K (\sigma_{ij}^\epsilon d_{ij}(v) - p^\epsilon \nabla.v) = 0, \forall 0 < \epsilon < \epsilon_0$$

and then

$$\lim_{\epsilon \to 0^+} -\nabla.\sigma^\epsilon + \nabla p^\epsilon = 0 \text{ in } [H^{-1}(\Omega)]^2. \ \square$$

Proof of case 2 (UCM model). For $a = 1$, the constitutive equation can be written as :

$$\sigma_{11} - 2\lambda\sigma_{12}u_{1,2} = 0, \sigma_{12} - \lambda\sigma_{22}u_{1,2} - u_{1,2} = 0, \sigma_{22} = 0,$$

which gives the classic relation

$$\sigma_{11} = 2\lambda u_{1,2}^2, \ \sigma_{12} = u_{1,2}, \ \sigma_{22} = 0. \tag{7}$$

Reasoning as in the previous case we then obtain the solution (3) of class $\mathcal{C}^1(\Omega)$. Now we consider the case of the existence of the weak solution. As previously, we set for u^ϵ :

$$u^\epsilon(x, y) = U_0(f_\epsilon + \frac{1 - |y|}{\epsilon} g_\epsilon, 0), U_0 = \frac{D}{2}$$

and we set for σ^ϵ and p^ϵ (see Fig. 1), with $c \in \mathbb{R}$ (with the parameter c, we obtain a weak solution defined up to a constant on Γ) :

$$\sigma_{11}^\epsilon = cU_0^2 g_\epsilon, \sigma_{12}^\epsilon = -sign(y)\frac{cU_0\epsilon}{2\lambda} g_\epsilon, \sigma_{22}^\epsilon = \frac{1}{\lambda}(\frac{c\epsilon^2}{2\lambda} - 1)g_\epsilon, p^\epsilon = \sigma_{22}^\epsilon + C_p.$$

The solution (4) is then obtained by taking the pointwise limit on Ω of $(\sigma^\epsilon, u^\epsilon, p^\epsilon)$ when ϵ tends to 0^+ and setting $C_\sigma = cU_0^2$. From the relation, for $y \neq \pm(1-\epsilon)$:

$$\sigma^\epsilon + \lambda B(u^\epsilon, \sigma^\epsilon) - 2d(u^\epsilon) = \begin{pmatrix} \sigma_{11}^\epsilon - 2\lambda\sigma_{12}^\epsilon u_{1,2}^\epsilon & \sigma_{12}^\epsilon - \lambda\sigma_{22}^\epsilon u_{1,2}^\epsilon - u_{1,2}^\epsilon \\ \sigma_{12}^\epsilon - \lambda\sigma_{22}^\epsilon u_{1,2}^\epsilon - u_{1,2}^\epsilon & \sigma_{22}^\epsilon \end{pmatrix} = \begin{pmatrix} 0 & 0 \\ 0 & \sigma_{22}^\epsilon \end{pmatrix},$$

we obtain

$$\lim_{\epsilon \to 0^+} \sigma^\epsilon + \lambda B(u^\epsilon, \sigma^\epsilon) - d(u^\epsilon) = 0 \ [L^1_{loc}(\Omega)]^4.$$

The limit of $-\nabla.\sigma^\epsilon + \nabla p^\epsilon$ to 0 in $[H^{-1}(\Omega)]^2$ when ϵ tends to 0^+ is treated as above. □

3. Numerical simulations. We use the symmetry of the flow, and we consider a flow in a domain of the form $\Omega_L =]0, L|\times]0, 1[$, with boundary conditions. We shall use $L = 8$ in the simulations. We consider the problem $(\mathcal{Q})$ posed on Ω_L :

$$(\mathcal{Q}) \qquad \sigma + \lambda B(u, \sigma) = 2d(u), -\nabla.\sigma + \nabla p = 0, \nabla.u = 0, \text{ in } \Omega_L,$$

we set $\Gamma^- = \{(x, y) \in \mathbb{R}^2, x = 0, y \in [0, 1]\}$ the inflow section of the boundary, $\Gamma^+ = \{(x, y) \in \mathbb{R}^2, x = L, y \in [0, 1]\}$ the outflow section of the boundary, $\Gamma_a = \{(x, y) \in \mathbb{R}^2, x \in [0, L], y = 0\}$ the axis of symmetry of the flow and $\Gamma_w = \{(x, y) \in \mathbb{R}^2, x \in [0, L], y = 1\}$ the wall of the flow over which the fluid velocity is zero (see Fig. 2). We denote by n the outward unit normal vector on the boundary of Ω and $t = (-n_2, n_1)$ the unit tangent. The velocity is imposed at the inflow boundary and to take into account the hyperbolic character of the constitutive equation, a boundary condition is imposed for σ on the boundary Γ^- (see [3]). Let $u_0 \in [H^1_{loc}(\Omega_L)]^2$ and $\sigma_0 \in [L^2(\Gamma^-)]^4$, with the condition of zero velocity at the wall and the condition on the axis of symmetry, the boundary conditions chosen for the problem $(\mathcal{Q})$ are then :

$$\sigma = \sigma_0 \text{ on } \Gamma^-, u = u_0 \text{ on } \Gamma^-, u = 0 \text{ on } \Gamma_w, \ u.n = 0 \text{ and } [(\sigma - pI).n].t = 0 \text{ on } \Gamma_a \ (\textit{Neumann}).$$

The Neumann condition on the axis of symmetry is satisfied by the solutions given in Proposition 1, with σ given by Eqns. (5) or (7) in the case of solutions of class $\mathcal{C}^1(\Omega)$: indeed, as $\sigma = 0$ on Γ_a, we then have $[(\sigma - pI).n].t = (pI.n).t = 0$.

At the exit of the flow, we have considered several types of conditions which give essentially the same results in the simulations :

• (DBC) : Dirichtlet conditions at the outflow : $u = u_0$ on Γ^+,

• (BC1) : Dirichtlet conditions at the outflow for $u.t$: $u_2 = 0$ on Γ^+, with Neumann boundary condition $[(\sigma - pI).n].n = 0$ on Γ^+,

• (BC2) : Neumann boundary condition at the outflow : $(\sigma - pI).n = 0$ on Γ^+.

The restrictions to $\bar{\Omega}_L$ of the solutions (σ, u, p) of the problem $(\mathcal{P})$ are solutions (in a formal sense for the weak solutions) of the problem $(\mathcal{Q})$ with Dirichtlet conditions (DBC) and the choice of the boundary conditions $(\sigma_0, u_0) = (\sigma, u)$. In the case of the UCM model, we will study the convergence of the approximated solutions when the couple (σ_0, u_0) is given by one of these solutions : in §3.3, the couple (σ_0, u_0) is given by the weak solution (2) or (4) and in §3.4, (σ_0, u_0) is given by the regular solution (3) and (7).

The FE formulations used for the approximation of the Problem $(\mathcal{Q})$ are, on the one hand, a modified SUPG type method with a splitting of the equations by a factor $\theta \in]0, 1]$ and on the other hand, an upwinding term coupled to a factor $\delta \geq 0$. This method allows to obtain FE convergence results in the case of a linear version of Maxwell's problem if we pick in the formulation

$$\theta = \frac{1}{1 + \delta},$$

(*cf.* [12]). For convenience, we will call this method θ-MSUPG method. On the other hand, we also compared the results with a SUPG type method, using the standard upwinding term $\delta u_h.\nabla\tau_h$, which we called θ-SUPG method.

Let us consider the case of Dirichlet conditions (DBC). With these conditions (DBC), the pressures are chosen in the space $M = L^2_0(\Omega_L)$ of functions of $L^2(\Omega_L)$ with zero mean value.

We assume that $u_0 = 0$ sur Γ_w and that the conditions of compatibility $\int_{\Gamma^- \cup \Gamma^+} u_0.n\, ds = 0$ and $u_0.n = 0$ on Γ_a are satisfied (it is not necessary that u_0 has zero divergence). In the sequel, we denote by $(\,,)$ the scalar product on $[L^2(\Omega_L)]^n$, $n \in \mathbb{N}$, and we denote $\langle \sigma, \tau \rangle_{\Gamma^-} = \int_{\Gamma^-} \sigma_{ij}\tau_{ij}|u_0.n|ds$. We set $T = \{\tau \in [H^1(\Omega_L)]^4, \tau \text{ symmetric}\}$, $X = \{v \in [H^1(\Omega_L)]^4, v = 0 \text{ on } \Gamma^- \cup \Gamma^+ \cup \Gamma_w, v.n = 0 \text{ on } \Gamma_a\}$.

We denote by $\{T_h \times X_h \times M_h\}_{h>0} \subset T \times X \times M$ a family of FE spaces. Let $\mu \geq 0$ be a parameter, the Problem $(\mathcal{Q})$ is then approximated by the following problem $(\mathcal{Q}_h)$ (as an indication we have kept in the formulation the term α which has the value $\alpha = 1$ in the simulations) :

θ-MSUPG Method

Find $(\sigma_h, u_h, p_h) \in T_h \times (u_0 + X_h) \times M_h$ *such that* $\forall (\tau, v, q) \in T_h \times X_h \times M_h$ *we have :*

$$(\mathcal{Q}_h) \begin{cases} (\sigma_h + \lambda B(u_h, \sigma_h), \tau + \delta\lambda B(u_h, \tau)) + \lambda(1+\delta)\langle \sigma_h, \tau \rangle_{\Gamma^-} \\ \qquad = 2\alpha(d(u_h), \tau + \delta\lambda B(u_h, \tau)) + \lambda(1+\delta)\langle \sigma_0, \tau \rangle_{\Gamma^-}, \\ \theta(\sigma_h, d(v)) + (1-\theta)(2\alpha d(u_h) - \lambda B(u_h, \sigma_h), d(v)) \\ +2(1-\alpha)(d(u_h), d(v)) - (p_h, \nabla.v) + \mu(\nabla.u_h, \nabla.v) = (f, v), \\ (\nabla.u_h, q) = 0. \end{cases}$$

For $\theta = 1$ and $\delta = 0$, we find a classical Galerkin method. On the other hand, we also used method of type θ-SUPG, where the upwinding term $\lambda B(u_h, \tau)$ in $(\mathcal{Q}_h)$ is replaced by the term $\lambda u_h \nabla.\tau$:

θ-SUPG Method

Find $(\sigma_h, u_h, p_h) \in T_h \times (u_0 + X_h) \times M_h$ *such that* $\forall (\tau, v, q) \in T_h \times X_h \times M_h$ *we have :*

$$(\mathcal{Q}'_h) \begin{cases} (\sigma_h + \lambda B(u_h, \sigma_h), \tau + \delta\lambda u_h \nabla.\tau) + \lambda(1+\delta)\langle \sigma_h, \tau \rangle_{\Gamma^-} \\ \qquad = 2\alpha(d(u_h), \tau + \delta\lambda u_h \nabla.\tau) + \lambda(1+\delta)\langle \sigma_0, \tau \rangle_{\Gamma^-}, \\ \theta(\sigma_h, d(v)) + (1-\theta)(2\alpha d(u_h) - \lambda B(u_h, \sigma_h), d(v)) \\ +2(1-\alpha)(d(u_h), d(v)) - (p_h, \nabla.v) + \mu(\nabla.u_h, \nabla.v) = (f, v), \\ (\nabla.u_h, q) = 0. \end{cases}$$

For $\theta = 1$, we find a classical SUPG method for the Maxwell model. When $\theta = 1$, the FE spaces must verify an inf-sup tensor-velocity condition so that problems $(\mathcal{Q}_h)$ or $(\mathcal{Q}'_h)$, for the approximation of the three-field Stokes problem obtained by setting $\lambda = 0$ in $(\mathcal{Q})$, are well-posed (*cf.* [4], [5],[9],[11]). Numerical results, to which we refer in the context of 3.1, using this type of FE are presented in [13], [14], [15]. The formulations of problems $(\mathcal{Q}_h)$ and $(\mathcal{Q}'_h)$ corresponding to the conditions (BC1) and (BC2) are obtained in a similar way by adapting the space X to the boundary conditions and taking the space $L^2(\Omega)$ as pressure space. In the case of the UCM model, we have obtained approximate solutions showing a slip at the wall, close to the weak solutions of Proposition 1, only with the θ-MSUPG method.

Let $c \geq 0$ be a parameter, the problem $(\mathcal{Q}_h)$ is solved by the following fixed point iteration : let $(\sigma_h^n, u_h^n, p_h^n) \in T_h \times (u_0 + X_h) \times M_h$ be given, then $(\sigma_h^{n+1}, u_h^{n+1}, p_h^{n+1}) \in T_h \times (u_0 + X_h) \times M_h$ is given by :

$$(\mathcal{FP}) \begin{cases} (\sigma_h^{n+1} + \lambda B(u_h^n, \sigma_h^{n+1}), \tau + \delta\lambda B(u_h^n, \tau)) + \lambda(1+\delta)\langle \sigma_h^{n+1}, \tau \rangle_{\Gamma^-} \\ \qquad = 2\alpha(d(u_h^{n+1}), \tau + \delta\lambda B(u_h^n, \tau)) + \lambda(1+\delta)\langle \sigma_0, \tau \rangle_{\Gamma^-}, \\ \theta(\sigma_h^{n+1}, d(v)) + (1-\theta)(2\alpha d(u_h^{n+1}) - \lambda B(u_h^n, \sigma_h^{n+1}), d(v)) \\ \quad +2(1-\alpha+c)(d(u_h^{n+1}), d(v)) - (p_h^{n+1}, \nabla.v) + \mu(\nabla.u_h^{n+1}, \nabla.v) \\ \qquad = (f, v) + 2c(d(u_h^n), d(v)) \\ (\nabla.u_h^{n+1}, q) = 0, \forall (\tau, v, q) \in T_h \times X_h \times M_h. \end{cases}$$

The c term allows us to improve, in certain cases and in a very significant manner, the convergence of the fixed point algorithm above. The fixed point used to solve problem $(\mathcal{Q}'_h)$ is analogous.

The domain Ω is equipped with a conforming triangulation $\{\mathcal{T}_h\}_{h>0}$ of triangles K. The computations are performed on different triangulations, on the mesh $\mathcal{M}_1$ and on the mesh $\mathcal{M}_2$ which is a refinement of this mesh (see Fig. 2 and also Fig. 14, lefts graphs, details of the meshes). The FE spaces used are the P_1-continuous FE space for the tensor and pressure approximation and the P_2-continuous FE space for the velocity approximation. To take into account the case $\theta = 1$, we will also use continuous finite element P_1-bubbles for the tensor approximation, with :

$$T_h = \{\tau \in [\mathcal{C}^0(\Omega_L)]^4,\ \tau_{|K} \in [P_1(K) \oplus b_4(K)]^4,\ \forall K \in \mathcal{T}_h\},$$

with $b_4(K) = \text{span}\{\lambda_1^2\lambda_2\lambda_3, \lambda_1\lambda_2^2\lambda_3, \lambda_1\lambda_2\lambda_3^2\}$, where $\{\lambda_i\}_{1\leq i\leq 3}$ is a set of barycentric coordinates of K.

In §3.4, we also considered a more regular and anisotropic mesh $\mathcal{M}_3$ (see Fig. 16) (with a P_1-continuous or P_2-continuous approximation of the tensors) in the context of a study of the stability of the regular Poiseuille flow (3), when this flow is a solution of the boundary problem $(\mathcal{Q})$ (UCM model).

To study the variations of the approximate solution close to the wall (see Fig. 5 and Fig. 9, the variations of the velocity), we set Δ_1 be the line $y = 47/48 \simeq 0.9792$ which intersects the horizontal edges of the first row of triangles of the mesh $\mathcal{M}_1$, by counting these triangles from the top of Ω_L (see Fig. 2 and Fig. 14, details of the mesh). In the same way, for the mesh $\mathcal{M}_2$, we denote by Δ_2 the corresponding line, which has for equation $y = \frac{1535}{1536} \simeq 0.99935$. The second row of triangles of the mesh $\mathcal{M}_2$ is bounded by Δ_2 and by the line Δ'_2 of equation $y = \frac{1534}{1536} \simeq 0.9987$.

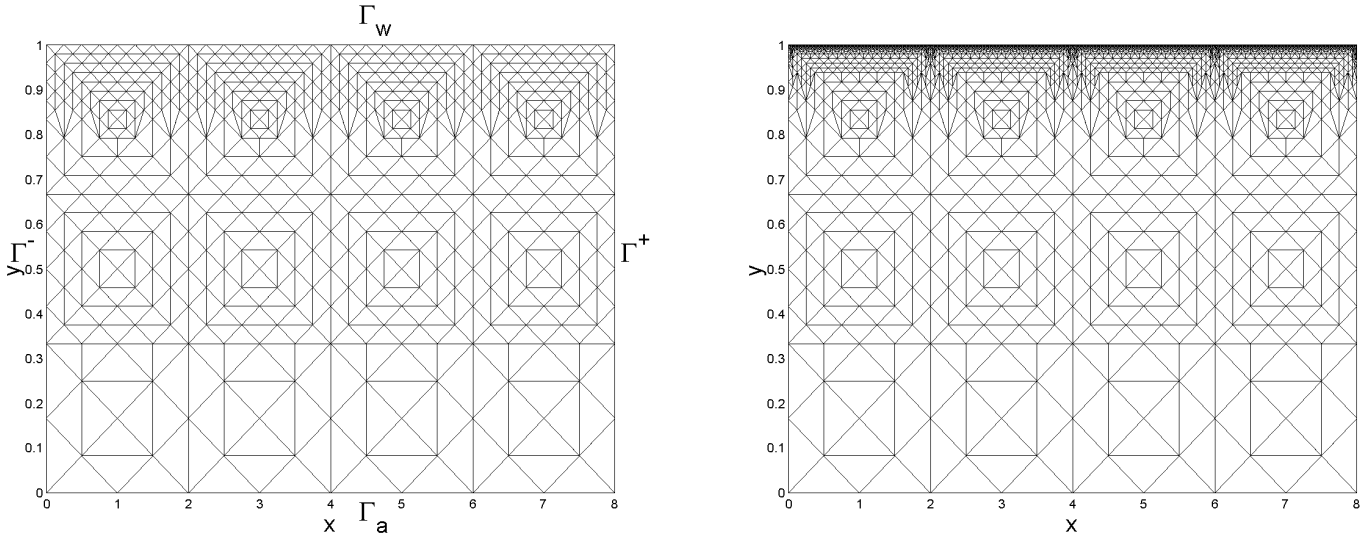

Fig. 2. Meshes $\mathcal{M}_1$ (992 triangles, 529 vertices) and $\mathcal{M}_2$ (9668 triangles, 5368 vertices), the mesh of the wall Γ_w of the flow has for respective sizes $h = \frac{1}{4}$ $(\mathcal{M}_1)$ and $h = \frac{1}{128}$ $(\mathcal{M}_2)$. On the mesh $\mathcal{M}_1$, the triangle T_1 located at the upper left-hand corner of Ω_L has for coordinates $(0,1), (\frac{1}{8}, \frac{47}{48}), (\frac{1}{4}, 1)$ and on the mesh $\mathcal{M}_2$, the triangle T_1 located at the upper left-hand corner of Ω_L has for coordinates $(0,1), (\frac{1}{256}, \frac{1535}{1536}), (\frac{1}{128}, 1)$. Number of unknowns for the $P_1^4 \times P_2^2 \times P_1$-continuous approximation : 6214 unknowns (Mesh $\mathcal{M}_1$) and 62278 unknowns (Mesh $\mathcal{M}_2$).

We study the role played by the weak solutions on the behaviour of the fixed point and the numerical solutions in several cases. In §3.3, we study the convergence of the approximated

solution to a weak solution on the whole domain. In §3.1, 3,2 and 3.4, in view to study the stabilization of approximate solutions towards a weak solution, we consider a median part of the flow and a median part of the boundary chosen in the following way. We set, for the study in the neighbourhood of the boundary Γ_w :

$$F = \{(x, y) \in \mathbb{R}^2, x \in [1, 7], y = 1\}$$

and we will study the behaviour on F of the extra-stress tensor and the pressure. We also set

$$F^\star = \{(x, y) \in \mathbb{R}^2, x \in [1, 7], y = 0.99\},$$

for the study of the velocity (which is zero on F) in the neighbourhood of Γ_w, with the following choice of norms, per unit length :

$$\|f\|_F = \frac{1}{6}\int_1^7 |f(x, 1)|\, dx, \|f\|_{F^\star} = \frac{1}{6}\int_1^7 |f(x, 0.99)|\, dx.$$

For the study on the domain Ω_L, we set A be the following domain obtained by taking a median part of Ω_L minus a strip of width 0.1 along Γ_w :

$$A = \{(x, y) \in \mathbb{R}^2, x \in [3, 6], y \in [0, 0.9]\},$$

with the choice of the norm

$$\|f\|_A = \int_A |f|.$$

In the case where the pressure is defined up to a given constant (case of the boundary conditions (DBC)), we will use the mean value of the pressure over A :

$$p_A \stackrel{\text{def}}{=} \frac{1}{mes(A)}\int_A p,$$

as well as its mean value over Ω_L :

$$\bar{p} \stackrel{\text{def}}{=} \frac{1}{mes(\Omega_L)}\int_{\Omega_L} p.$$

In §3.1, in the case of the COM model and in §3.2 in the case of the UCM model, we study the approximation of the Problem $(\mathcal{Q})$ with boundary conditions of type (BC2) and we study the stabilization of the solutions of the approximated problems $(\mathcal{Q}_h)$ or $(\mathcal{Q}'_h)$ towards a weak solution. In §3.3, we study the approximation of problem $(\mathcal{Q})$ with (DBC) boundary conditions given by a weak solution. In the case of the UCM model, when λ is sufficiently large, the approximate solution given by the θ-MSUPG method converges, with the mesh refinement towards the weak solution, whereas in the case of the SUPG or θ-SUPG method, the fixed point diverges, with a method that does not capture the solution. In §3.4, for the UCM model, we study the approximation of the problem $(\mathcal{Q})$, in the case where the solution is given by the Poiseuille flow of class $\mathcal{C}^1(\Omega)$ given by (3) and (7). As λ increases, the fixed point method applied to the SUPG or θ-SUPG method starts to diverge while the θ-MSUPG method gives an approximate solution that stabilizes towards a weak solution, with a convergence curve close to a plateau phase. This process occurs also when the solution of the problem $(\mathcal{Q})$ belongs to the FE space and is then a solution of the problem $(\mathcal{Q}_h)$ or $(\mathcal{Q}'_h)$ (this is possible due to rounding errors).

The norm used to study the convergence of the iterative method $(\mathcal{FP})$ is the following energy norm :

$$\|(\sigma, u, p)\| = [\int_\Omega \sigma_{ij}\sigma_{ij} + d_{ij}(u)d_{ij}(u) + p^2]^{\frac{1}{2}}$$

and we denote by

$$U_h^n = (\sigma_h^n, u_h^n, p_h^n)$$

the n^{th} iterate of the fixed-point iteration $(\mathcal{FP})$. In a part of the results listed below, the convergence curves obtained are not all complete, in particular because of the computation times which can be long. Indeed, some of these curves have convergence rates close to 1, which leads to very long computation times (for example, see Fig. 10, where the convergence curve is plotted for 355729 iterations). For example, on the mesh $\mathcal{M}_2$, the average computation time of an iteration is about 250 s., which leads to computation times of the order of 1 year for 126000 iterations. Some calculations have been accelerated by parallelizing the assembly of FEM in the limit of the calculation possibilities. Other curves present phases which are close to a plateau. During these phases, we can however observe a significant variation of the energy norm as shown in Fig. 9 (right hand graph) or readjustments of the solution in areas of discontinuity as in Fig. 9 (left hand graph). In the case of a flow in a 4 :1 contraction, we were able to obtain solutions with slip at the downstream wall of the flow as well as completed convergence on meshes of the same size at the downstream wall as those used here. It seems that the corner singularity would more easily cause the slip, which would then improve the convergence of the fixed point (see [15]).

3.1. Corotational Maxwell model. Let denote by (σ^f, u^f, p^f) the weak solution given by Eqn. (2). We consider the problem $(\mathcal{Q})$ with a boundary conditions of type (BC2). We set as a boundary condition on Γ^- : $u_0(x, y) = 4(1 - y^2)$ and $\sigma_0 = 2d(u_0)$ (Poiseuille flow of a fluid governed by the Stokes equations with a flow rate of value $\frac{16}{3}$). There is no condition imposed for u on the outflow boundary Γ^+.

The Neumann condition $(\sigma - pI).n = 0$ imposed on Γ^+ allows to determine the integration constant of p. For the constant C_p of the weak solution (*cf.* Eqn. (2)), as $\sigma^f = 0$ on Ω, this gives $p^f = C_p = 0$.

For this flow, the Weissenberg number is given by $We = |\frac{\partial u_0}{\partial y}(x, 1)|\lambda = 8\lambda$. The flow rate is then $D = \frac{16}{3}$, which gives the value of $U_0 = \frac{8}{3}$ in the expression of the weak solution given by Eqn. (2).

For $a = 0$, the critical value λ_c (*cf.* Proposition 1. Case 1, a)) is given by $\lambda_c = \frac{3}{8} - \frac{3}{32}\pi \simeq 0.08047$, which gives a critical Weissenberg number of $We = 0.6438$.

For $\lambda < \lambda_c$, the component u_1 of the solution approximated by the methods θ-SUPG and θ-MSUPG stabilizes in the middle of the flow towards the regular solution u_1 of Proposition 1, Eqn. (1) (*cf.* [14], [15], Fig. 3.2).

A simulation result for a slightly higher value than λ_c, given by $\lambda = 0.0825$, is shown in Fig. 3-5 and Table 1. The method used is the θ-MSUPG method. We choose, as in §3.2 and §3.4, as the initial starting iterate in the fixed point iteration $(\mathcal{FP})$, the solution $(\sigma_h^0, u_h^0, p_h^0)$ of the Stokes Problem obtained for $\lambda = 0$. In §3.3, this is an interpolant in $u_0 + X_h$ of the weak solution which will be chosen as starting point

We observe, downstream of the domain and on the downstream wall of the flow, a stabilization of the approximate solution towards the weak solution (see Figs. 3, 4). It is worth noting that the Galerkin method without upwinding obtained by setting $\delta = 0$ in $(\mathcal{Q}_h)$, including the classical Galerkin method obtained for $\theta = 1$, as well as the method θ-SUPG, with or without splitting, *i.e.* with $\theta = 1$, allow to obtain similar results (*cf.* [14], [15]). When $\theta = 1$, these

results are obtained with the use of FE spaces that satisfy the tensor-velocity inf-sup condition which allows to stabilize the approximation of the Stokes problem obtained by setting $\lambda = 0$ in $(\mathcal{Q})$ (*cf.* [5],[9],[11]). In this sense, the regular solution is stable for these FE methods.

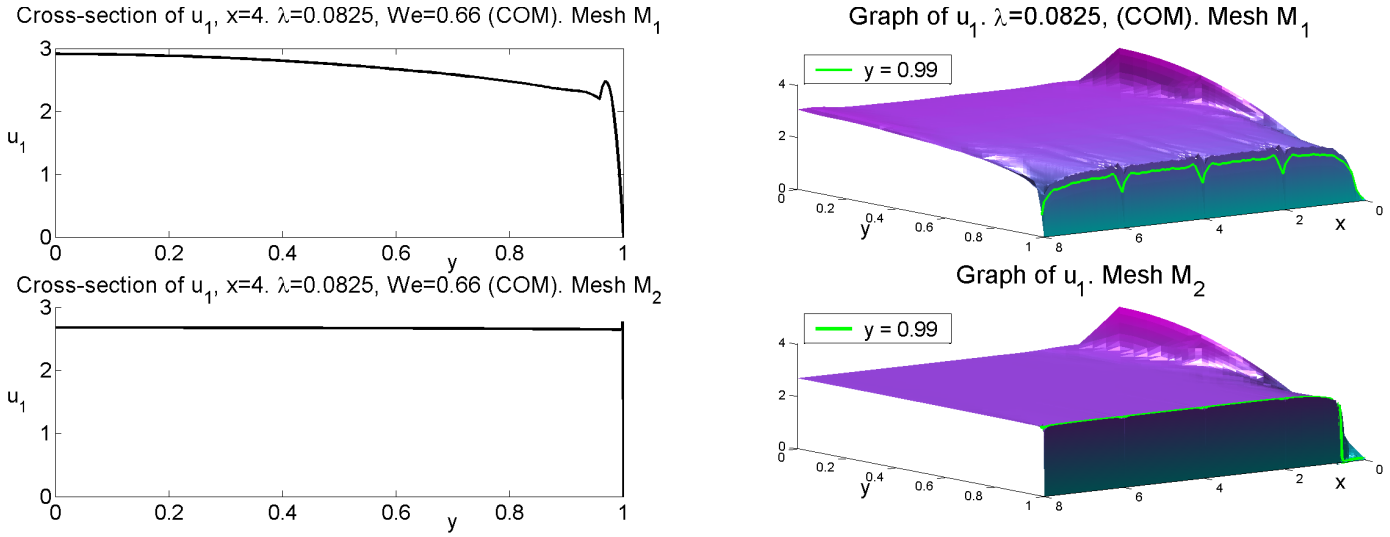

Fig. 3. Corotational Maxwell model. Left graphs : cross-section of u_1 along the line $x = 4$ (u is the approximate solution). Right hand graphs : graph of u_1 (opposite view) and graph of the curve $x \to u_1(x, 0, 99)$, $x \in [0, 8]$. COM Model, $a = 0$, $\lambda = 0.0825$, $We = 8\lambda = 0.66$, boundary conditions (BC2). Parameters of $(\mathcal{FP})$: $(\theta, \delta, \mu, c) = (\frac{10}{11}, \frac{1}{10}, 2, 0)$. MSUPG term of upwinding : $\delta\lambda B(u_h^n, \tau)$. FE space : $P_1^4 \times P_2^2 \times P_1$-continuous. Results on meshes $\mathcal{M}_1$ and $\mathcal{M}_2$.

Figure 4 gives the graphs of the approximate solution σ_{11} obtained on meshes $\mathcal{M}_1$ and $\mathcal{M}_2$ (see the graphs on the left), as well as cross-sectional views of σ_{11} and σ_{22} in the neighbourhood of Γ_w (see graphs on the right). On Γ_w, the component σ_{11} takes values close to $\frac{1}{\lambda} \simeq 12.1212$ and σ_{22} takes values close to $-\frac{1}{\lambda}$. Tab. 1 gives the mean values taken by σ on the median part F of Γ_w.

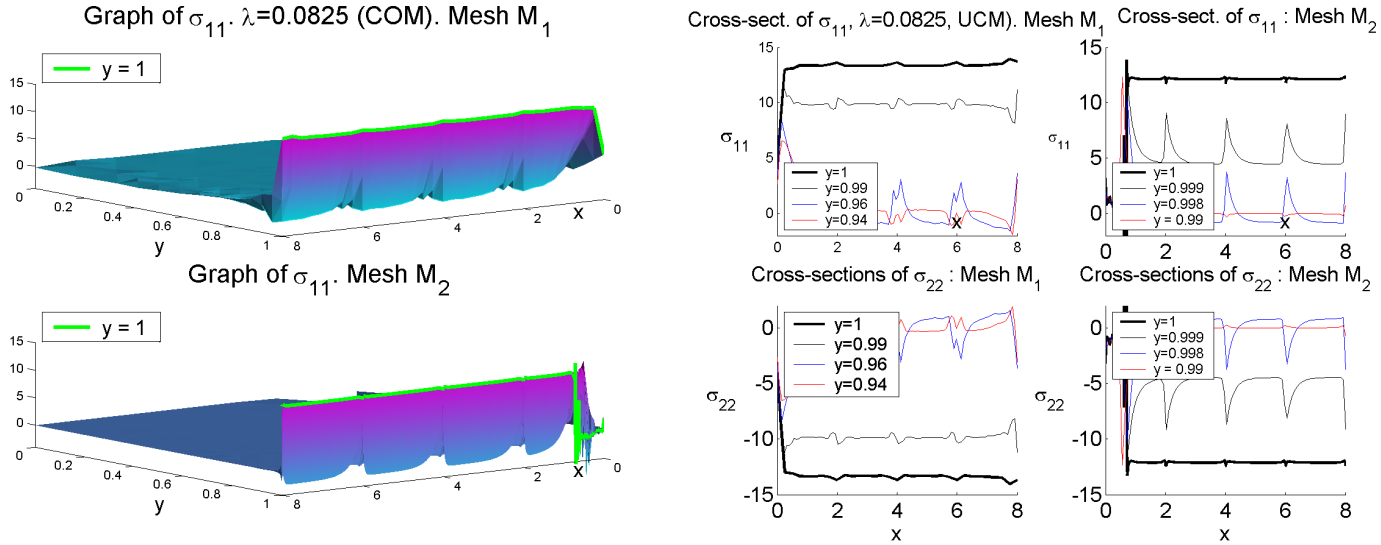

Fig. 4. Corotational Maxwell model (continuation of Fig. 3). Left graphs : graph of the function σ_{11} obtained on the meshes $\mathcal{M}_1$ and $\mathcal{M}_2$ and graph of the curve $x \to \sigma_{11}(x, 1)$, $x \in [0, 8]$. Right hand graphs : cross-sections of σ_{11} and σ_{22} along the lines $y = 0.94, 0.96, 0.99$ (thin lines) and $y = 1$ (thick line) for the mesh $\mathcal{M}_1$ and the lines $y = 0.99, 0.998, 0.999$ (thin lines) and $y = 1$ (thick line) for the mesh $\mathcal{M}_2$.

In Table 1, we look at the stabilization of the approximate solution towards the weak solution on the line segments $F \subset \Gamma_w$, $F^\star \subset \overline{\Omega}_L$ and on the downstream part of the flow $A \subset \Omega_L$. We

observe, with the mesh refinement, the convergence of the approximate solution (σ, u, p) to the weak solution (σ^f, u^f, p^f) on the rectangle A, as well as the convergence of (σ, p) to (σ^f, p^f) on the line segment F and the convergence of the velocity u to u^f on the line segment $F^\star$. We set, for $U = (\sigma, u, p)$:

$$\|U\|_{F,F^\star} = \|\sigma_{11}\|_F + \|\sigma_{12}\|_F + \|\sigma_{21}\|_F + \|\sigma_{22}\|_F + \|u_1\|_{F^\star} + \|u_2\|_{F^\star} + \|p\|_F,$$
$$\|U\|_A = \|\sigma_{11}\|_A + \|\sigma_{12}\|_A + \|\sigma_{21}\|_A + \|\sigma_{22}\|_A + \|u_1\|_A + \|u_2\|_A + \|p\|_A.$$

Let $U^f = (\sigma^f, u^f, p^f)$ be the weak solution and let U^i be the approximate solution obtained on the mesh $\mathcal{M}_i$, we have the ratios :

$$\frac{\|U^f - U^1\|_{F,F^\star}}{\|U^f - U^2\|_{F,F^\star}} = 26.09, \ \frac{\|U^f - U^1\|_A}{\|U^f - U^2\|_A} = 24.11,$$

close to the ratio 32 of the size of the mesh $\mathcal{M}_1$ on the side Γ_w to the corresponding size of the mesh $\mathcal{M}_2$. This gives an indication of convergence towards the weak solution, on a restricted part of the domain, of order $\mathcal{O}(h^{0.94})$ and $\mathcal{O}(h^{0.92})$, where h is the size of the mesh of the wall Γ_w.

θ-MSUPG Met., FE $P_1^4 \times P_2^2 \times P_1$-cont., $(\theta, \delta, \mu, c) = (\frac{10}{11}, \frac{1}{10}, 2, 0)$, $a = 0$, $\lambda = 0.0825$, (BC2).						
Mesh	$\frac{1}{6}\int_1^7 \sigma_{11}(x,1)\,dx$	$\frac{1}{6}\int_1^7 \sigma_{12}(x,1)\,dx$	$\frac{1}{6}\int_1^7 \sigma_{22}(x,1)\,dx$	$\frac{1}{6}\int_1^7 u_1(x,0.99)\,dx$	$\frac{1}{6}\int_1^7 u_2(x,0.99)\,dx$	$\frac{1}{6}\int_1^7 p(x,1)\,dx$
$\mathcal{M}_1$	13.39	-0.77	-13.38	1.96	-0.0002	-7.75
$\mathcal{M}_2$	12.14	-0.02	-12.11	2.64	0.0002	-12.15
$^{(a)}L^1$-norm	$\|\sigma_{11}-\sigma_{11}^f\|_F$	$\|\sigma_{12}-\sigma_{12}^f\|_F$	$\|\sigma_{22}-\sigma_{22}^f\|_F$	$\|u_1-u_1^f\|_{F^\star}$	$\|u_2-u_2^f\|_{F^\star}$	$\|p-p^f\|_F$
$\mathcal{M}_1$	1.27	0.77	1.26	0.71	0.0043	4.37
$\mathcal{M}_2$	0.028	0.016	0.025	0.028	0.0008	0.24
$^{(b)}L^1$-norm	$\|\sigma_{11}-\sigma_{11}^f\|_A$	$\|\sigma_{12}-\sigma_{12}^f\|_A$	$\|\sigma_{22}-\sigma_{22}^f\|_A$	$\|u_1-u_1^f\|_A$	$\|u_2-u_2^f\|_A$	$\|p-p^f\|_A$
$\mathcal{M}_1$	0.16	1.81	0.16	0.44	0.0175	16.07
$\mathcal{M}_2$	0.008	0.076	0.008	0.018	0.0017	0.66

Table 1. Corotational Maxwell model. Convergence study. $a = 0$, $\lambda = 0.0825$, $\frac{1}{\lambda} = 12.1212$, $We = 0.66$. The triple (σ, u, p) is the solution of the approximate problem $(\mathcal{Q}_h)$ and (σ^f, u^f, p^f) is the weak solution of the Proposition 1, Eqn. (2), with $U_0 = \frac{8}{3}$ and $C_p = 0$. $^{(a)}$ L^1-norms reduced to the unit, on a median part of the wall of the flow : $\|f\|_F = \frac{1}{6}\int_1^7 |f|(x,1)\,dx$, or on a line segment close to the wall of the flow : $\|f\|_{F^\star} = \frac{1}{6}\int_1^7 |f(x,0.99)|\,dx$, $^{(b)}$ L^1-norm on a median part of the domain $\|f\|_A = \int_A |f|$. Number of iterations : 956 $(\mathcal{M}_1)$ and 41891 $(\mathcal{M}_2)$, relative error between the last two iterates : $2.05e-015$ $(\mathcal{M}_1)$ and $7.53e-015$ $(\mathcal{M}_2)$.

Other choices of conditions on σ at the inflow boundary, for example by choosing σ given by the relation (5), also lead to solutions with slip for $\lambda > \lambda_c$ (see Fig. 5, the curves of convergence obtained for this example).

The first graph in Fig. 5 shows an enlargement of the cross-section along the line $x = 5$ of the approximate solution u_1 obtained on the mesh $\mathcal{M}_2$, with a representation of the mesh in the neighbourhood of this line. Approximately, the function $u_1(5, y)$ takes the value U_0 for $0 \leq y \leq 0.99935$, then after an oscillation, decreases in an affine way towards the zero value. Thus, the variation of u_1 occurs on the last row of triangles, at the level of Δ_2. Let $\epsilon = \frac{1}{1536}$,

the velocity profile is then close to that of the solution u^ϵ defined in §2 (see also Fig. 1, the graph of u^ϵ for $\epsilon = \frac{1}{3}$).

The second graph of Fig. 5 gives the curves of convergence in norm of the energy of the fixed point $(\mathcal{FP})$ (curve of the logarithm of the relative error, as a function of the number of iterations). We observe a linear convergence with a convergence rate that increases with the mesh refinement. The last graph of Fig. 5 is an enlargement of the previous one, on which we have added curves of convergences obtained for $\lambda = 0.08 < \lambda_c$ and $\lambda = 0.0825 > \lambda_c$, with the inflow boundary conditions for σ given by Eqn. (5). For $\lambda = 0.0825 > \lambda_c$, the curves show a plateau phase which corresponds to the appearance of the wall slip during the fixed point process. For $\lambda = 0.08 < \lambda_c$, there is no occurrence of wall slip and no corresponding plateau phase.

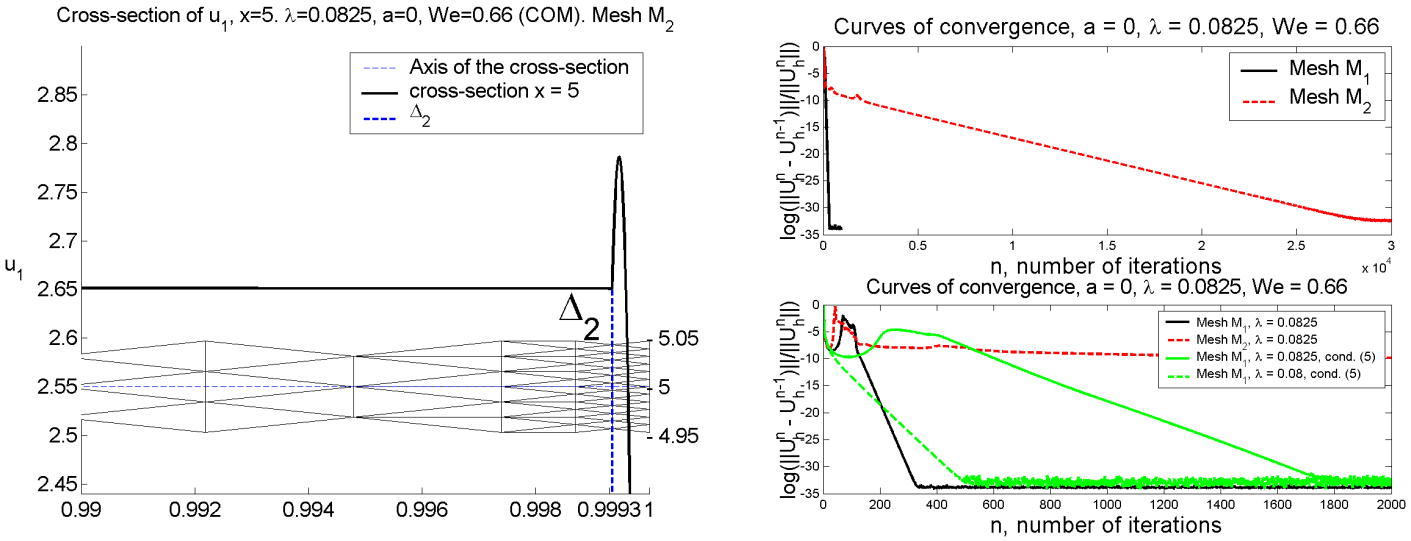

Fig. 5. Corotational Maxwell model (continuation of Fig. 4). Left graph : cross-section of u_1 along $x = 5$ and drawing of an enlargement of the mesh $\mathcal{M}_2$ in the neighbourhood of $x = 5$. Upper right-hand graph : curves of convergence on the meshes $\mathcal{M}_1$ and $\mathcal{M}_2$, number of iterations : 956 $(\mathcal{M}_1)$, 41891$(\mathcal{M}_2)$. Lower right-hand graph, enlargement of the curves in the figure above and addition of the curves of convergence obtained on the mesh $\mathcal{M}_1$ with the condition σ_0 given by the relation (5).

3.2. Upper convected Maxwell model. We denote by (σ^f, u^f, p^f) the weak solution given by Eqn. (4). The chosen boundary conditions are identical to those of the previous case, with the pressure p^f selected to be 0 in Ω_L. Compared to the COM model, the situation is different in the case of the convected Maxwell model ($a = 1$), for which there is no loss of existence of a Poiseuille flow of class $\mathcal{C}^1$, regardless of the flow rate D imposed. On the other hand the weak solution of Proposition 1 gives a set of solutions of σ_{11} defined up to a constant C_σ.

When λ increases in the numerical simulations, the fixed point scheme $(\mathcal{FP})$ starts, in general, to converge to a regular solution, Then, with the growth of λ, in the case of SUPG or θ-SUPG methods, the fixed point scheme begins to diverge. For the θ-MSUPG methods and for values of λ that remain bounded, a wall slip appears on the flow wall Γ_w and the velocity stabilizes downstream of the domain towards the velocity u^f given by the weak solution of the Proposition 1 (see Fig. 6).

For example, on the mesh $\mathcal{M}_1$, in the case of the θ-MSUPG method, a flow with wall slip appears from $\lambda \simeq 0.25$. We observe this slip up to values of $\lambda = 0.375$, accompanied by a slowing down of the convergence speed of the fixed point. For all these simulations, we used the following parameters $(\theta, \delta, \mu, c) = (\frac{10}{11}, \frac{1}{10}, 2, 1)$. In the case of the θ-SUPG method, with

these parameters and the same mesh, the fixed point converges up to $\lambda = 0.3$ towards a regular solution (convergence is obtained after about 600 iterations), then it diverges from $\lambda = 0.3125$. However, for this value of λ, the fixed point remains convergent if we sufficiently increase the value of c (which generally has the effect of increasing the rate convergence of the fixed point). Thus, for $c = 100$, convergence is obtained after about 40000 iterations.

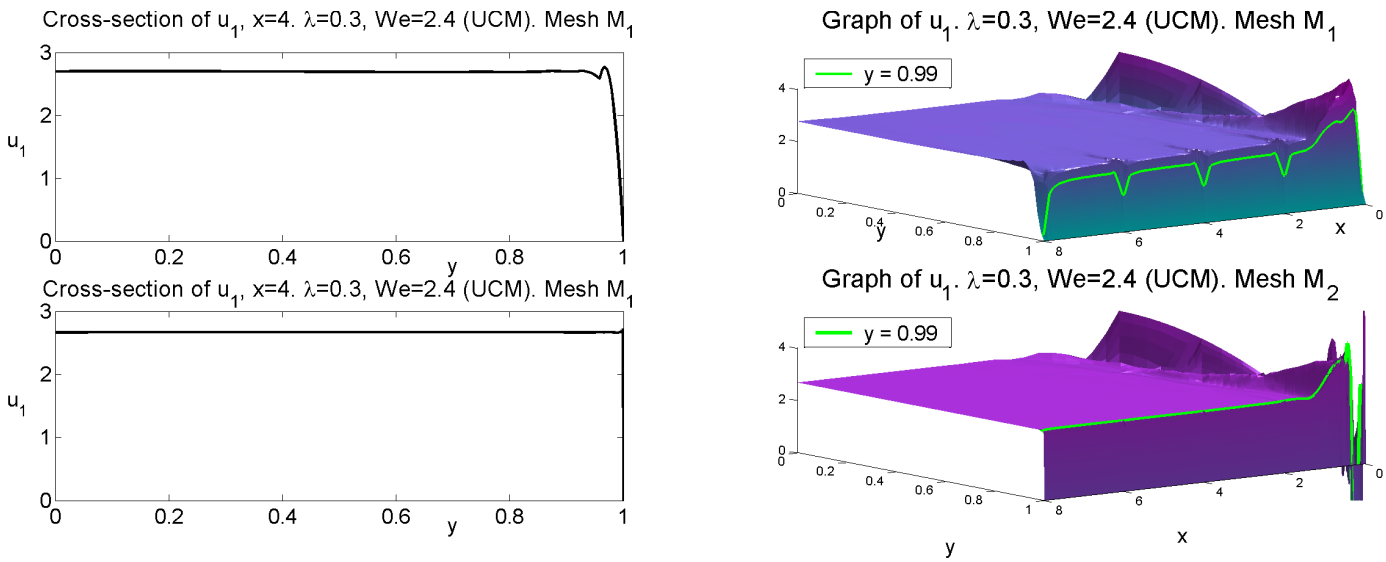

Fig. 6. Upper convected Maxwell model. Left graphs : cross-section of u_1 along the line $x = 4$ (u is the approximate solution). Right hand graphs : graph of u_1 (opposite view) and graph of the curve $x \to u_1(x, 0, 99)$, $x \in [0, 8]$. UCM model, $a = 1$, $\lambda = 0.3$, $We = 8\lambda = 2.4$, boundary conditions (BC2). Parameters of $(\mathcal{FP})$: $(\theta, \delta, \mu, c) = (\frac{10}{11}, \frac{1}{10}, 2, 1)$. MSUPG term of upwinding : $\delta\lambda B(u_h^n, \tau)$. FE space : $P_1^4 \times P_2^2 \times P_1$-continuous. Results on meshes $\mathcal{M}_1$ and $\mathcal{M}_2$.

A simulation result for a value of $\lambda = 0.3$, with the use of the θ-MSUPG method, is described in Figs. 6-9 and in Table 2. Fig. 6 describes the component u_1 of the velocity obtained on the meshes $\mathcal{M}_1$ and $\mathcal{M}_2$. The Figs. 7 and 8 describe the extra-stress-tensor, with, in Fig. 7 (upper right-hand graph), cross sections of σ_{11} including a section along the F_β segment that we define below and that corresponds to a minimum for σ_{11}. In these figures and Table 2, we observe a stabilization of the approximated solution towards the weak solution downstream of the domain and at the downstream wall of the flow (the weak solution is defined up to an additive coefficient C_σ in the definition of the weak solution σ_{11}). We precise the choice of C_σ used in Table 2 below. On the middle part F of the wall of the flow, we observe for the norm $\|\|_F$, a convergence of σ_{12} towards 0 and a convergence of σ_{22} towards $-\frac{1}{\lambda}$ (see also Fig. 8, left-hand graphs). Tab. 2 gives the mean values taken by σ on the median part F of Γ_w. Oscillations appear in the neighbourhood of the boundary Γ_w on the component σ_{11} of the extra-stress tensor (see Fig. 7, lefts graphs and upper right-hand graphs). However, these oscillations disappear with the use of more regular meshes (*cf.* §3.3.4) as with the mesh $\mathcal{M}_1'$ (see Fig. 14, left graphs). On Fig. 7 we have represented with a dashed line a section of σ_{11} obtained on this mesh, with a smoothing of the oscillations. The curves of convergence are given in Fig. 9.

There exists an infinite number of weak solutions defined up to the constant C_σ, which is the value taken on the boundary Γ_w by the weak solution σ_{11}^f. In the numerical simulations, the component σ_{11} of the extra-stress tensor seems to stabilize well, in mean, on the part F of the boundary, around a constant value that we denote $C_{\sigma,h}$. This value $C_{\sigma,h}$ depends on the mesh, with an indetermination on the eventual limit of $C_{\sigma,h}$ when the mesh size tends to 0. By averaging over F, we have : $C_{\sigma,h} = 5.1714 \pm 1.1137$ (deviation in norm $\|.\|_F$) on the mesh $\mathcal{M}_1$ and $C_{\sigma,h} = -2.0094 \pm 0.3278$ on the mesh $\mathcal{M}_2$, the thinnest mesh (*cf.* Tab. 2).

For $0 \leq b \leq 1$, let $F_b = \{(x, y), x \in [1, 7], y = b\}$ be the line segment of Ω_L located on the line $y = b$ parallel to the wall of the flow. We are looking for β that minimizes on F_b the mean

value of σ_{11} given by $\frac{1}{6}\int_1^7 \sigma_{11}(x,b)\,dx$. On the mesh $\mathcal{M}_1$, we find $\beta = \frac{47}{48} \pm 5e-4 \simeq 0.9792$, $\frac{1}{6}\int_1^7 \sigma_{11}(x,\beta)\,dx = -0.3752$ (see Fig. 7, the plot of u_1 along the line $y=\beta$). The line segment F_β is thus included in the line Δ_1. On the mesh $\mathcal{M}_2$, we find $\beta = 1 \pm 2e-5$, $\frac{1}{6}\int_1^7 \sigma_{11}(x,\beta)\,dx = -2.0094$ (see Fig. 7). The line segment F_β is thus, this time, included in the boundary Γ_w. This would numerically give the following hypothesis of determination of σ_{11} on the boundary Γ_w, when the size h of the mesh of Γ_w tends to 0, with $\beta = \beta_h$ depending on h :

$$(8) \qquad \int_1^7 \sigma_{11}(x,\beta_h)\,dx = \inf_{b\in[0,1]} \int_1^7 \sigma_{11}(x,b)\,dx, \ \lim_{h\to 0}\beta_h = 1, \ \lim_{h\to 0}\frac{1}{6}\int_1^7 \sigma_{11}(x,\beta_h)\,dx = -\frac{1}{\lambda}.$$

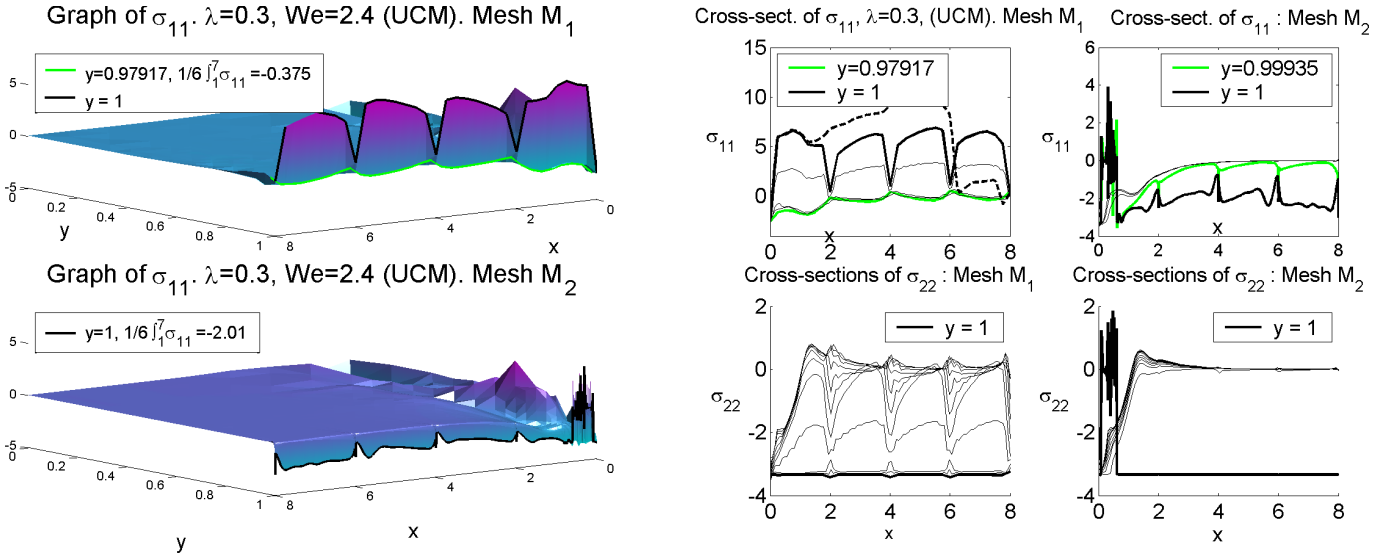

Fig. 7. Upper convected Maxwell model (continuation of Fig. 6). Left graphs : graph of σ_{11} (opposite view) and graph of σ_{11} along the line $y=1$ and along the line $y=\beta$ for the mesh $\mathcal{M}_1$ (on this mesh, $\beta \neq 1$). Right graphs : cross-sections of σ_{11} along the lines $y = 0.97, 0.98, 0.99$ (thin lines), $y=1$, $y=\frac{47}{48}$ (mesh $\mathcal{M}_1$) and $y=\frac{1535}{1536}$ (mesh $\mathcal{M}_2$) (thick lines) and cross-sections of σ_{22} along the lines $y = 0.9, 0, 91\cdots, 0.99$ (thin lines) and $y=1$ (thick line). On the mesh $\mathcal{M}_1$: $\beta = \frac{47}{48} \sim 0.9792$ with the mean value $\frac{1}{6}\int_1^7 \sigma_{11}(x,\beta)\,dx = -0.3752$. On the mesh $\mathcal{M}_2$: $\beta = 1$ with the mean value $\frac{1}{6}\int_1^7 \sigma_{11}(x,\beta)\,dx = -2.0094$. Dashed curves : cross-sectional view along the line $y=1$ of the FEM solution σ_{11} obtained on the mesh $\mathcal{M}_1'$.

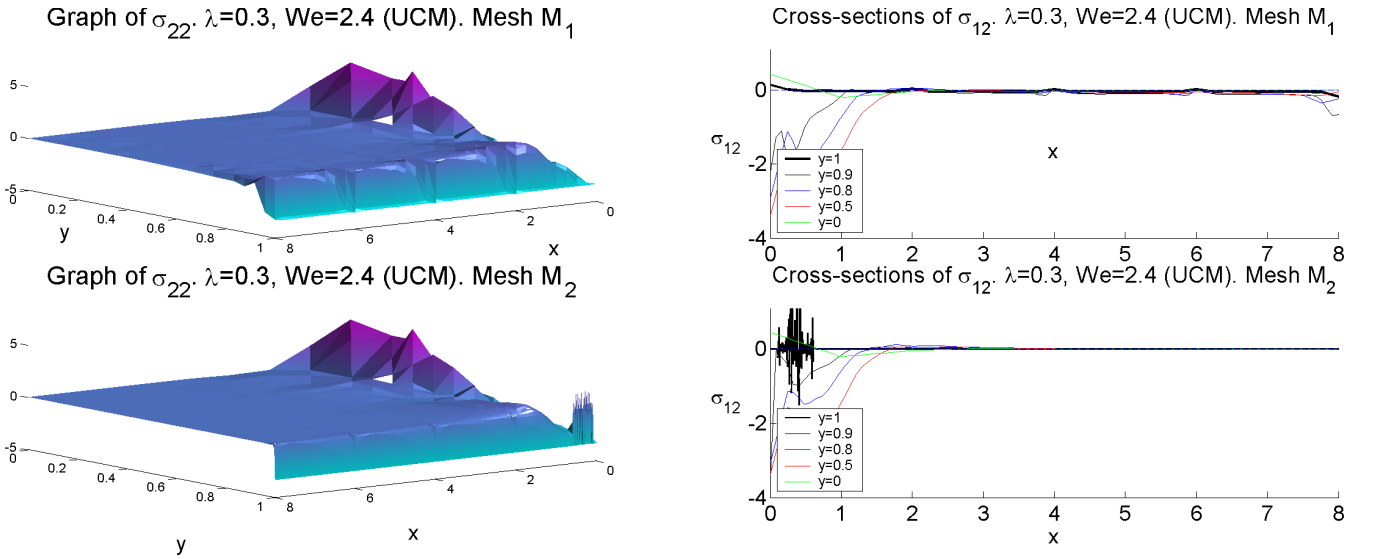

Fig. 8. Upper convected Maxwell model (continuation of Figures 6-7). Left graphs : graph of σ_{22} (opposite view). Right graphs : cross-section of σ_{12} along the lines $y = 0, 0.2, 0.5, 0.9$ (thin lines) and $y=1$ ((thick line).

For the one-dimensional flow, we have the relation $\sigma_{11} - 2\lambda\sigma_{12}u_{1,2} = 0$, with σ_{12} close to 0 and with $u_{1,2}$ that tends to $-\infty$ on Γ_w. When $u_{1,2} < 0$, with this previous relation, σ_{11} is then of opposite sign to the sign of σ_{12}. In Table 2 and Fig. 8 (right graphs), we can see that the component σ_{12}, negative in mean on Γ_w when solving on the mesh $\mathcal{M}_1$, becomes positive in mean on Γ_w with the use of the mesh $\mathcal{M}_2$, which corresponds well to the change of sign observed on $C_{\sigma,h}$. This relation may explain in part the numerical instabilities observed on σ_{11} (cf Fig. 7), with the possibility of a convergence of the absolute value of $C_{\sigma,h}$ towards $\frac{1}{\lambda}$.

With the notations of §3.1 for the norms $\|.\|_A$ and $\|.\|_{F,F^\star}$, let $U^f = (\sigma^f, u^f, p^f)$ be the weak solution, let U^i be the solution obtained on the mesh $\mathcal{M}_i$. We have the ratios :

$$\frac{\|U^f - U^1\|_{F,F^\star}}{\|U^f - U^2\|_{F,F^\star}} = 3.85, \frac{\|U^f - U^1\|_A}{\|U^f - U^2\|_A} = 8.78,$$

this gives respectively an indication of convergence towards the weak solution, on a restricted part of the domain, of order $\mathcal{O}(h^{0.39})$ and $\mathcal{O}(h^{0.63})$, where h is the size of the mesh of Γ_w. This convergence result is to be modulated by the fact that we choose as the value of σ_{11}^f at the wall, the mean value $C_{\sigma,h}$ obtained on each mesh (indetermination of the constant C_σ).

θ-MSUPG Met., FE $P_1^4 \times P_2^2 \times P_1$-cont., $(\theta, \delta, \mu, c) = (\frac{10}{11}, \frac{1}{10}, 2, 1)$, $a = 1$, $We = 2.4$, (BC2).						
Mesh	$\frac{1}{6}\int_1^7 \sigma_{11}(x,1)\,dx$	$\frac{1}{6}\int_1^7 \sigma_{12}(x,1)\,dx$	$\frac{1}{6}\int_1^7 \sigma_{22}(x,1)\,dx$	$\frac{1}{6}\int_1^7 u_1(x,0.99)\,dx$	$\frac{1}{6}\int_1^7 u_2(x,0.99)\,dx$	$\frac{1}{6}\int_1^7 p(x,1)\,dx$
$\mathcal{M}_1$	5.1714	-0.0244	-3.3562	2.1833	-0.0007	-2.5859
$\mathcal{M}_2$	-2.0094	0.0009	-3.3334	2.6884	-0.0009	-3.1281
L^1-norm	$\|\sigma_{11}-\sigma_{11}^f\|_F$	$\|\sigma_{12}-\sigma_{12}^f\|_F$	$\|\sigma_{22}-\sigma_{22}^f\|_F$	$\|u_1-u_1^f\|_{F^\star}$	$\|u_2-u_2^f\|_{F^\star}$	$\|p-p^f\|_F$
$\mathcal{M}_1$	1.1137	0.0283	0.0228	0.4898	0.0064	0.7474
$\mathcal{M}_2$	0.3278	0.0009	0.0001	0.0232	0.0014	0.2781
L^1-norm	$\|\sigma_{11}-\sigma_{11}^f\|_A$	$\|\sigma_{12}-\sigma_{12}^f\|_A$	$\|\sigma_{22}-\sigma_{22}^f\|_A$	$\|u_1-u_1^f\|_A$	$\|u_2-u_2^f\|_A$	$\|p-p^f\|_A$
$\mathcal{M}_1$	0.0603	0.1113	0.0586	0.0597	0.0105	1.5266
$\mathcal{M}_2$	0.0539	0.0317	0.0407	0.0042	0.0025	0.0562

Table 2. Upper convected Maxwell model. Convergence study. The notations are those in Table 1. The triple (σ, u, p) is the solution of the approximate problem $(\mathcal{Q}_h)$ and (σ^f, u^f, p^f) is the weak solution of the Proposition 1, Eqn. (4), with $U_0 = \frac{8}{3}$ and $C_p = 0$. On the boundary Γ_w, $\sigma_{11}^f = C_\sigma$ is estimated by the mean value $C_{\sigma,h} = \frac{1}{6}\int_1^7 \sigma_{11}(x,1)\,dx$. $\frac{1}{\lambda} = 3.333$. Number of iterations 32605 ($\mathcal{M}_1$) and 423438 ($\mathcal{M}_2$), relative error between the last two iterates : $7.38e{-}015$ ($\mathcal{M}_1$) and $3.54e-006$ ($\mathcal{M}_2$).

We notice that the velocity is very sensitive to the geometric irregularities of the mesh located at the points $(2,1)$, $(4,1)$, $(6,1)$ (see Fig. 6, upper right-hand graph, the graph and the cross-section along the line $y = 0.99$ of the solution u_1 obtained on the mesh $\mathcal{M}_1$). The variations of u_1 at these points are particularly amplified on σ_{11} (see Fig. 7). The question of a more regular mesh is addressed in the next § 3.3. For example, the meshes $\mathcal{M}_1'$ and $\mathcal{M}_2'$ shown in Fig. 14 allow to relatively smooth the irregularities that appear on the curves of Fig. 11 (see Fig. 15, the results on these meshes). As mentioned above, Fig. 7 (upper right-hand graph) shows a cross-section of the function σ_{11} obtained with the mesh $\mathcal{M}_1'$, with a decrease of the oscillations on the first three quarters of the wall.

Other inflow boundary conditions on σ, such as $\sigma = 0$, or (BC1) boundary conditions, give similar results to those of this §. The choice of an inflow boundary conditions on σ given by the

relation (7) (regular Poiseuille flow), also leads to solutions with wall slip, but for higher values of λ. This case is discussed in Section 4, in the framework of the Dirichtlet conditions (DBC).

The Fig. 9 (left graph) shows a cross-sectional view of the velocity obtained for $x = 5$. We observe, after a large number of iterations, an adjustment of the solution to the graph of u_1^ϵ, with $\epsilon = \frac{1}{1536}$, while the curve of convergence is close to a plateau phase.

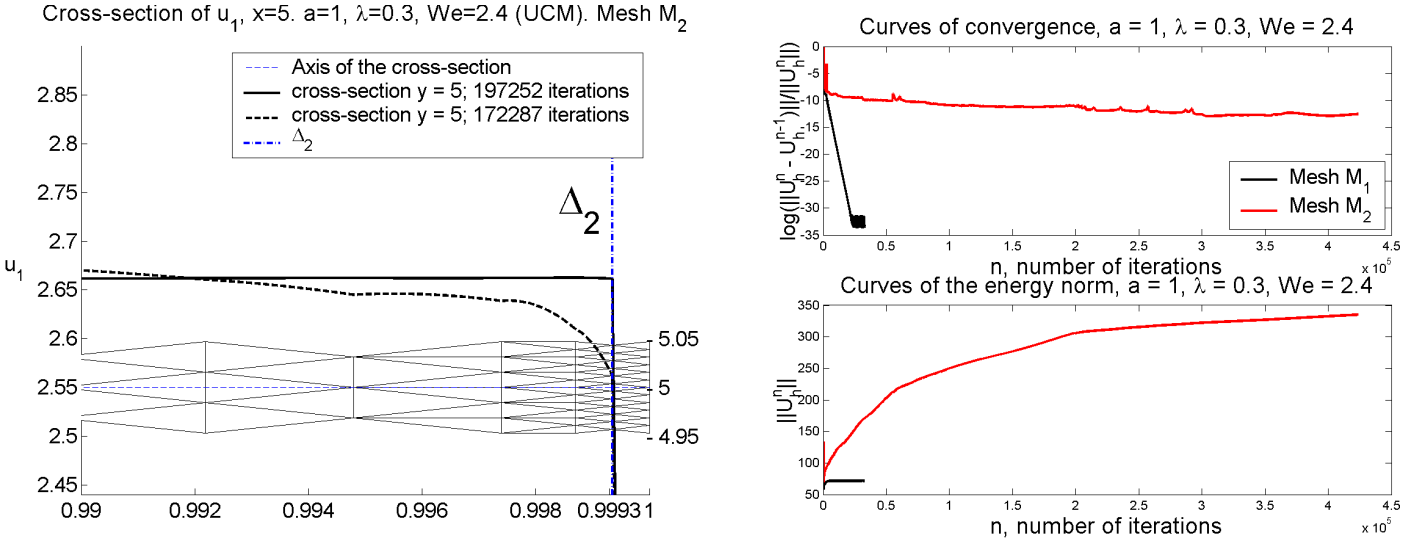

Fig. 9. Upper convected Maxwell model (continuation of Figs. 6-8). Left graph : cross-section of u_1 along $x = 5$ and drawing of an enlargement of the mesh $\mathcal{M}_2$ in the neighbourhood of $x = 5$. On this graph, Δ_2 is the line of equation $y = \frac{1535}{1536}$. Upper right-hand graph : curves of convergence. Lower right-hand graph : curves of the energy norms of the iterates. Number of iterations : 32605 ($\mathcal{M}_1$), 423438 ($\mathcal{M}_2$).

3.3. Inflow and outflow boundary condition on the velocity of crenel-type function (weak solution). Let denote by (σ^f, u^f, p^f) the weak solution given by Proposition 1, Eqn. (2) (COM model case) or Eqn. (4) (UCM model case). We study the problem $(\mathcal{P})$ with boundary conditions given by the weak solutions σ^f and u^f (the profile of the velocity is then a function of crenel-type). We first study the case of UCM model for high values of λ before examining the case of the COM model in §3.3.2, the case of small values of λ in §3.3.3 and the case of the influence of the mesh in §3.3.4.

3.3.1. Inflow and outflow condition of crenel-type (weak solution, UCM model). We consider the case of the upper convected Maxwell model. We denote by (σ^f, u^f, p^f) the weak solution given by Eqn. (4). We choose constant inflow and outflow velocity boundary condition *i.e.* we set as boundary condition $u_0 = u^f$, where u^f is the weak solution given by Eqn. (4), with $U_0 = \frac{8}{3}$. We choose as inflow boundary condition on Γ^- for $\sigma : \sigma_0 = \sigma^f = 0$. The initial iterate chosen for the fixed point $(\mathcal{FP})$ is $(\sigma_h^0, u_h^0, p_h^0) = (0, u^i, 0)$, where $u^i \in X_h$ is the interpolant of the weak solution u^f, *i.e.* u^i is equal to 0 on the degrees of freedom located on the boundary Γ_w and is equal to $\frac{8}{3}$ on the other degrees of freedom.

For this type of problem, the pressure is defined up to a constant, the chosen pressure is the pressure whose mean is zero. For the weak solution, the constant C_p is chosen such that $p^f = C_p$ has zero mean value, which thus gives $C_p = 0$. Let p be the pressure solution of the approximate problem $(\mathcal{Q}_h)$ (numerically, p is obtained by setting $p = 0$ on a degree of freedom of the FE space), we set $\tilde{p} = p - \bar{p}$ the approximate pressure of zero mean. To study the convergence of the approximate pressure, we compare $\tilde{p}$ to the weak solution p^f. The mean value of $\tilde{p}$ at the wall is estimated by $\frac{1}{8}\int_0^8 \tilde{p}(x,1), dx = \frac{1}{8}\int_0^8 p(x,1)\, dx - \bar{p}$. On the boundary Γ_w, σ_{11}^f is defined up to a constant C_σ, in the convergence study in Table 3, $\sigma_{11}^f = C_\sigma$ is estimated by the mean value $C_{\sigma,h} = \frac{1}{8}\int_0^8 \sigma_{11}(x,1)\, dx$.

For comparison purposes, we have kept the value $We = 8\lambda$, although $|u_{1,2}|$ is infinite at the wall of the flow (in fact $u_{1,2}(x,.)$ is a Dirac function). In the rest of this paragraph, we present the simulation results obtained for $\lambda = 2$. In the case of the θ-MSUPG method, we see the convergence of the approximate velocity to the weak solution (see Fig. 10, left graphs). On the mesh $\mathcal{M}_1$, the convergence of the fixed point method ($\mathcal{FP}$) is obtained for the choice $c = 0$ (see Fig. 10, right-hand graphs), with an approximate solution close to the weak solution. For $c = 1$, as well as on the mesh $\mathcal{M}_2$, the convergence curves are not completed, with a fixed point which converges slowly. However, we note a stabilization of the energy norm curves (see Fig. 14) as well as the values in Table 3 which remain stable during the iterative process, and which show a convergence towards the weak solution.

In general, small values of c improve the convergence rate of the fixed point, when it converges. When the fixed point is unstable for small values of c, then larger values of c can improve its convergence.

When using the θ-SUPG method or the SUPG method (with continuous FE of type P_1-bubbles, for the approximation of tensors, as in [14]), the fixed point diverges for various values of c as $c = 1, 100$ (see Fig. 10, last graph, the curves of convergence obtained on the mesh $\mathcal{M}_1$, for the value $c = 100$). During the iterative process, the fixed point iterate u_h^n, initialized at the interpolate of the weak solution, gradually moves away from it before diverging.

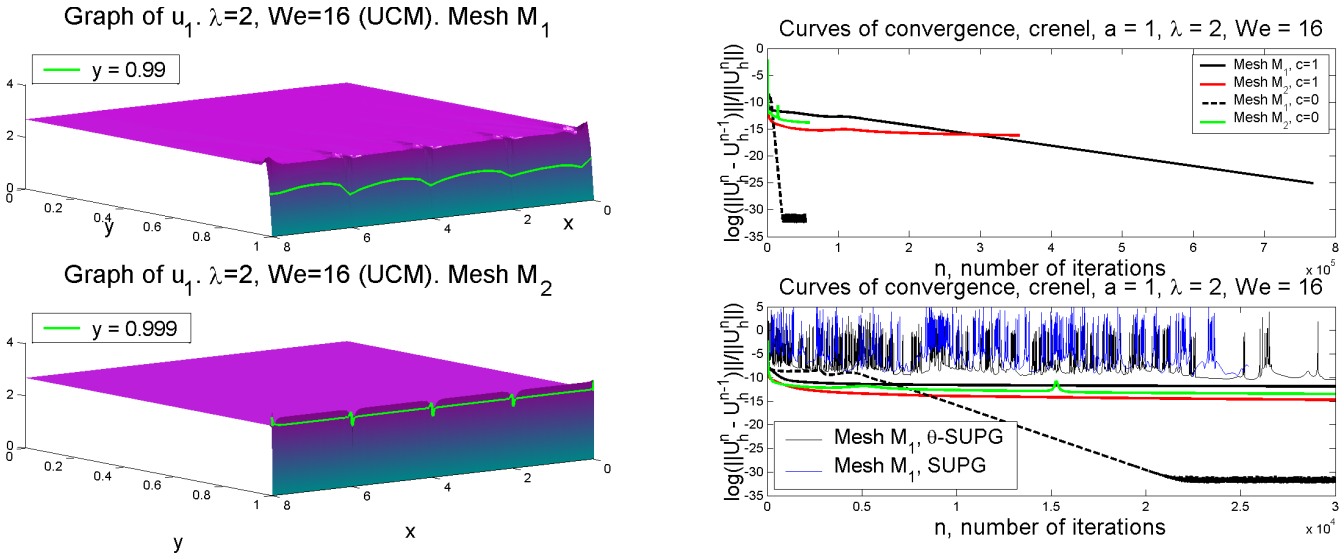

Fig. 10. Upper convected Maxwell model (§3.3. "Crenel"), the flow given by the weak solution is imposed in inflow and outflow. Left graphs : graphs of u_1. UCM model, $a = 1$, $\lambda = 2$, $We = 8\lambda = 16$, boundary conditions (DBC). Parameters : $(\theta, \delta, \mu, c) = (\frac{10}{11}, \frac{1}{10}, 2, 1)$. MSUPG term of upwinding : $\delta\lambda B(u_h^n, \tau)$. FE space : $P_1^4 \times P_2^2 \times P_1$-continuous. Results on meshes $\mathcal{M}_1$ and $\mathcal{M}_2$. Upper right-hand graph : corresponding curves of convergence obtained for $c = 1$, with the number of iterations : 769015 ($\mathcal{M}_1$), 355729 ($\mathcal{M}_2$) and curves of convergence obtained for $c = 0$. Lower right-hand graph : enlargement of the for curves of the upper right graph. Addition of the curves of convergence obtained for the θ-SUPG method and the SUPG method (approximation with the FE $P_1 \oplus$ *bubbles*-continuous for the tensors) with the value $c = 100$ in the fixed point ($\mathcal{FP}$), the convergence is not obtained on these curves.

For $0 \leq b \leq 1$, let $F_b' = \{(x,y), x \in [0,8], y = b\}$ be the line segment of Ω_L located on the line $y = b$. We are looking for β that minimizes on F_b' the mean value of σ_{11} given by $\frac{1}{8}\int_0^8 \sigma_{11}(x,b)\,dx$. On the mesh $\mathcal{M}_1$, we find $\beta = 1$, we have therefore $F_\beta' = \Gamma_w$ and $\frac{1}{8}\int_0^8 \sigma_{11}(x,\beta)\,dx = -0.2807$. On the mesh $\mathcal{M}_2$, we find $\beta = \frac{1534}{1536} \sim 0.9987$, $\frac{1}{6}\int_0^8 \sigma_{11}(x,\beta)\,dx = -0.2998$ (see Fig. 11, right graphs) and $F_\beta' \subset \Delta_2'$. On the boundary Γ_w, the function σ_{11} takes at its extremities the values

$\sigma_{11}(0,1) = -0.4112$ and $\sigma_{11}(8,1) = -0.4937$, close to $-\frac{1}{\lambda}$, and has the maximum value -0.0098.

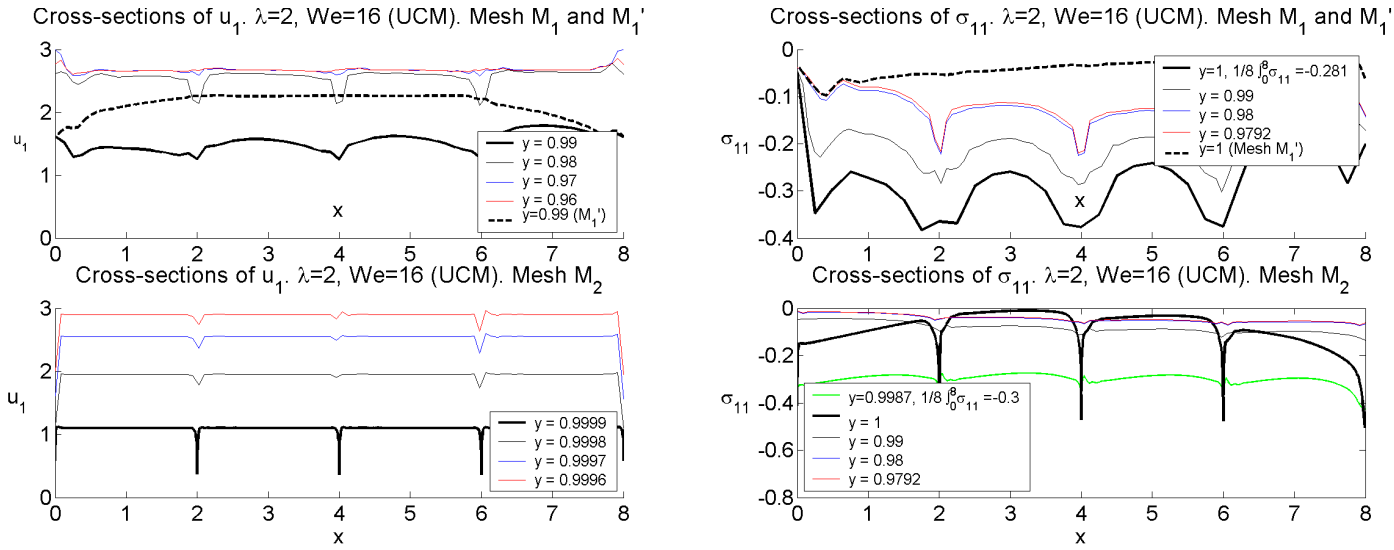

Fig. 11. Upper convected Maxwell model, §3.3, "Crenel" (continuation of Fig. 10). Left graphs : cross-section of u_1 along the lines $y = 0.96, 0.97, 0.98$ (thin line) and $y = 0.99$ (thick line) for the mesh $\mathcal{M}_1$ and $y = 0.9996, 0.9997, 0.9998$ (thin line) and $y = 0.9999$ (thick line) for the mesh $\mathcal{M}_2$. Right graphs : cross-section of σ_{11} along the lines $y = \frac{47}{48}, 0.98, 0.99$ (thin line), $y = 1$, and for the mesh $\mathcal{M}_2$, $y = \frac{1534}{1536}$ (thick line). On the mesh $\mathcal{M}_1$: $\beta = 1$, mean value $\frac{1}{8}\int_0^8 \sigma_{11}(x,\beta)\,dx = -0.2807$ and on the mesh $\mathcal{M}_2$: $\beta = \frac{1534}{1536} \sim 0.9987$, mean value $\frac{1}{8}\int_0^8 \sigma_{11}(x,\beta)\,dx = -0.2998$. Graphs above, dashed curves : cross-section of u_1 along the line $y = 0.99$ and cross-section of σ_{11} along the line $y = 1$ where (σ, u, p) is the FEM solution obtained on the mesh $\mathcal{M}_1'$, for comparison with the results obtained on the mesh $\mathcal{M}_1$ (see also Fig. 15).

We observe in Figs. 10 and 12 (lefts graphs), the convergence of the velocity towards the weak solution. It appears a loss of convergence in norm $L^\infty(\Omega_L)$ on the boundary Γ_w (see Fig. 12), similar to the Gibbs phenomenon.

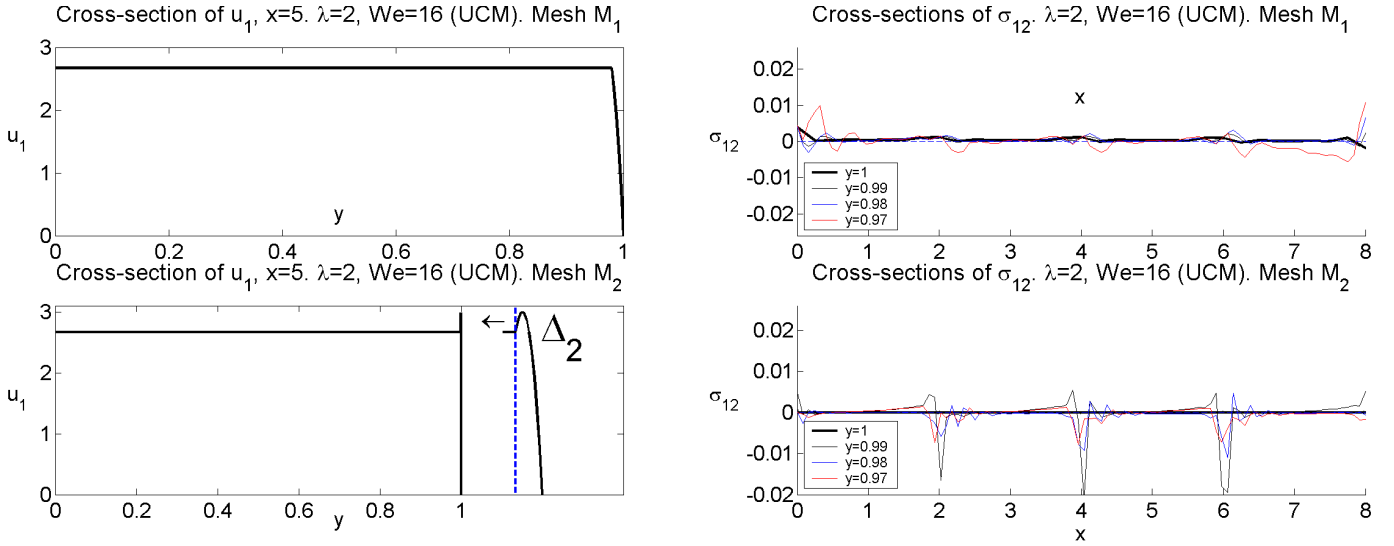

Fig. 12. Upper convected Maxwell model, §3.3, "Crenel" (continuation of Figures 10-11). Left graphs : cross-sections of u_1 along the line $x = 5$, and in the case of the mesh $\mathcal{M}_2$, enlargement of the graph for $y \in [0.999, 1]$, Right graphs : cross-sections of σ_{12} along the lines $y = 0.97, 0.98, 0.99$ (thin line) and $y = 1$ (thick line).

In Table 3, since the weak solution is the solution of the boundary problem, we have taken the norms over the whole domain, with the norms per unit length : $|f|_1 = \frac{1}{8}\int_1^8 |f|(x,1)\,dx$

and $|f|_{1^\star} = \frac{1}{8}\int_1^8 |f(x,0.99)|\,dx$, and with the norm $\|f\|_1 = \int_{\Omega_L} |f(x)|$. We observe the mesh convergence of the finite element method with the convergence of the approximate solution towards the weak solution. We set, for $U = (\sigma, u, p)$:

$$\|U\|_{1,1^\star} = |\sigma_{11}|_1 + |\sigma_{12}|_1 + |\sigma_{21}|_1 + |\sigma_{22}|_1 + |u_1|_{1^\star} + |u_2|_{1^\star} + |p|_1,$$
$$\|U\|_1 = \|\sigma_{11}\|_1 + \|\sigma_{12}\|_1 + \|\sigma_{21}\|_1 + \|\sigma_{22}\|_1 + \|u_1\|_1 + \|u_2\|_1 + \|p\|_1.$$

Let $U^f = (\sigma^f, u^f, p^f)$ be the weak solution and let U^i be the approximate solution obtained on the mesh $\mathcal{M}_i$. We have the ratios :

$$\frac{\|U^f - U^1\|_{1,1^\star}}{\|U^f - U^2\|_{1,1^\star}} = 9.03, \frac{\|U^f - U^1\|_1}{\|U^f - U^2\|_1} = 6.63,$$

This gives an indication of convergence towards the weak solution of order $\mathcal{O}(h^{0.64})$ and $\mathcal{O}(h^{0.55})$, where h is the size of the wall Γ_w. As in §3.2, the component σ_{11} of the extra-stress tensor is close to a constant value $C_{\sigma,h}$, on the whole boundary Γ_w (cf Fig. 11), with however irregularities. We obtain $C_{\sigma,h} = -0.2807 \pm 0.0510$ on the mesh $\mathcal{M}_1$ (deviation in norm $|.|_1$) and $C_{\sigma,h} = -0.0855 \pm 0.0539$ on $\mathcal{M}_2$ (*cf.* Tab. 3). In the case of the mesh $\mathcal{M}_2$, the component σ_{11} is more regular on the line Δ_2' than on Γ_w, with a quasi-constant value (see Fig. 11, lower right-hand graph) given by $\frac{1}{8}\int_0^8 |\sigma_{11}(x,\beta)|\,dx = -0.2998 \pm 0.0205$. We have, on the mesh $\mathcal{M}_1$:

$$\beta = 1, \frac{1}{8}\int_0^8 |\sigma_{11}(x,\beta) + \frac{1}{\lambda}|\,dx = 0.2193 \text{ and on } \Delta_1 : \frac{1}{8}\int_0^8 |\sigma_{11}(x, \frac{47}{48}) + \frac{1}{\lambda}|\,dx = 0.3748$$

and, on the mesh $\mathcal{M}_2$:

$$\beta = \frac{1534}{1536}, \frac{1}{8}\int_0^8 |\sigma_{11}(x,\beta) + \frac{1}{\lambda}|\,dx = 0.2002 \text{ and on } \Gamma_w : \frac{1}{8}\int_0^8 |\sigma_{11}(x,1) + \frac{1}{\lambda}|\,dx = 0.4145,$$

which gives an eventual mesh convergence of σ_{11} towards $-\frac{1}{\lambda}$ in the sense of (8), but this time on the whole boundary :

$$(8') \qquad \int_0^8 \sigma_{11}(x,\beta_h)\,dx = \inf_{b\in[0,1]} \int_0^8 \sigma_{11}(x,b)\,dx,\ \lim_{h\to 0}\beta_h = 1, \lim_{h\to 0}\frac{1}{8}\int_0^8 \sigma_{11}(x,\beta_h)\,dx = -\frac{1}{\lambda}.$$

θ-MSUPG method, $(\theta,\delta,\mu,c) = (\frac{10}{11}, \frac{1}{10}, 2, 1)$, $a = 1$, $\lambda = 2$, $\frac{1}{\lambda} = 0.5$, (DBC).

Mesh	$\frac{1}{8}\int_0^8 \sigma_{11}(x,1)\,dx$	$\frac{1}{8}\int_0^8 \sigma_{12}(x,1)\,dx$	$\frac{1}{8}\int_0^8 \sigma_{22}(x,1)\,dx$	$\frac{1}{8}\int_0^8 u_1(x,0.99)\,dx$	$\frac{1}{8}\int_0^8 u_2(x,0.99)\,dx$	$\frac{1}{8}\int_0^8 \tilde{p}(x,1)\,dx$
$\mathcal{M}_1$	-0.2807	0.0005	-0.5003	1.5254	1.9307e-006	-0.4295
$\mathcal{M}_2$	-0.0855	4.9692e-006	-0.5000	2.6658	-6.7215e-008	-0.4538
L^1-norm	$\lvert\sigma_{11}-\sigma_{11}^f\rvert_1$	$\lvert\sigma_{12}-\sigma_{12}^f\rvert_1$	$\lvert\sigma_{22}-\sigma_{22}^f\rvert_1$	$\lvert u_1-u_1^f\rvert_{1^\star}$	$\lvert u_2-u_2^f\rvert_{1^\star}$	$\lvert\tilde{p}-p^f\rvert_1$
$\mathcal{M}_1$	0.0510	0.0005	0.0007	1.1413	0.0019	0.1103
$\mathcal{M}_2$	0.0539	6.1129e-006	2.6195e-006	0.0038	0.0015	0.0854
L^1-norm	$\lVert\sigma_{11}-\sigma_{11}^f\rVert_1$	$\lVert\sigma_{12}-\sigma_{12}^f\rVert_1$	$\lVert\sigma_{22}-\sigma_{22}^f\rVert_1$	$\lVert u_1-u_1^f\rVert_1$	$\lVert u_2-u_2^f\rVert_1$	$\lVert\tilde{p}-p^f\rVert_1$
$\mathcal{M}_1$	0.0962	0.0158	0.2865	0.2531	0.0302	0.4159
$\mathcal{M}_2$	0.0270	0.0039	0.0482	0.0089	0.0044	0.0717

Table 3. Upper convected Maxwell model, §3.3, "Crenel" (continuation of Figures 10-12). Convergence study. The triple (σ, u, p) is the solution of the approximate problem $(\mathcal{Q}_h)$ and (σ^f, u^f, p^f) is the weak solution of the Proposition 1, Eqn. (4), with $U_0 = \frac{8}{3}$. On the boundary Γ_w, $\sigma_{11}^f = C_\sigma$ is estimated by the mean value $\frac{1}{8}\int_0^8 \sigma_{11}(x,1)\,dx$, $C_p = 0$. $\frac{1}{\lambda} = \frac{1}{2}$. Number of iterations : 769015 ($\mathcal{M}_1$) and 355729 ($\mathcal{M}_2$), relative error between the last two iterates : $1.29e-011$ ($\mathcal{M}_1$) and $9.47e-008$ ($\mathcal{M}_2$).

3.3.2. Case of the COM model. We consider the corotational model with $\lambda = 2$. We denote by (σ^f, u^f, p^f) the weak solution given by Eqn. (2). We give in Fig. 13, the graph of the approximate velocity and pressure obtained on the mesh $\mathcal{M}_1$. We observe the convergence of the approximated solution to the weak solution. For the pressure, the mean value of $\tilde{p}$ on Γ_w is $\frac{1}{8}\int_0^8 \tilde{p}(x,1)\,dx = -0.5026$, close to the value $-\frac{1}{\lambda}$ of the weak solution p^f at the wall, with the deviation in norm $|p - p^f|_1 = 0.1357$. We note an oscillation of the pressure at the point $(0,0)$. This type of oscillation, amplified by the mesh refinement, occurs also for the UCM model : in this case the solution $\tilde{p}$ converges in norm $L^1(\Omega_L)$ towards $\tilde{p}$ (*cf.* Table 4), but not in norm $L^\infty(\Omega_L)$.

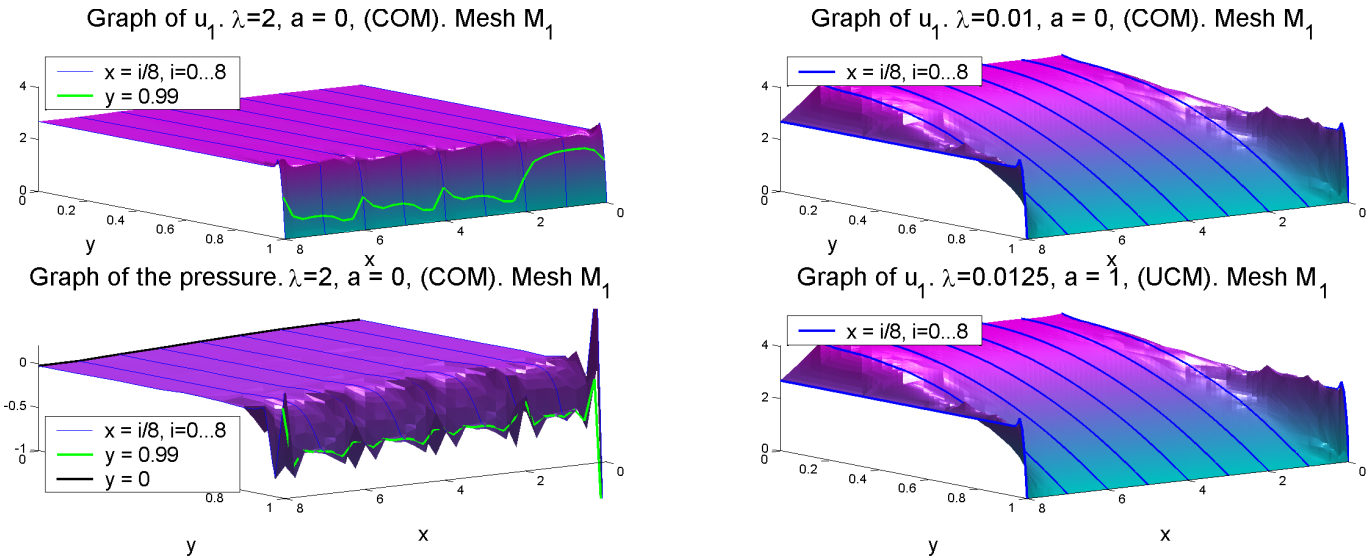

Fig. 13. Corotational and Upper convected Maxwell model, §3.3, "Crenel" (continuation of Figures 10-12). Left graphs, COM model, $\lambda = 2$. Stabilization towards the weak solution, graphs of velocity and pressure $\tilde{p}$. Right graphs, COM and UCM models : stabilization towards the Poiseuille flow of class $\mathcal{C}^1$ with $\lambda = 0.01$ for the corotational model and $\lambda = 0.0125$ for the upper convected Maxwell model. Parameters of $(\mathcal{FP})$: $(\theta, \delta, \mu, c) = (\frac{10}{11}, \frac{1}{10}, 2, 1)$. Mesh $\mathcal{M}_1$. Opposite angle of view.

3.3.3. Case of the small values of λ. We consider the problem with crenel-type boundary conditions on the velocity, for small values of λ. On the mesh $\mathcal{M}_1$, with $\lambda = 0.0125$ for the COM model and for $\lambda = 0.01$ for the UCM model, the SUPG, θ-SUPG and θ-MSUPG methods give solutions that stabilize, on part of the domain, towards the Poiseuille flow of class $\mathcal{C}^1$, for both types of models (see Fig. 13, right graphs). On the refined mesh $\mathcal{M}_2$, the COM model gives similar results, with, for the θ-MSUPG and SUPG methods (with an almost completed convergence for the latter), a regular solution similar to that of Fig 13. The θ-SUPG method gives an intermediate solution between the regular solution and the weak solution. In the case of the UCM model, the fixed point, associated to the SUPG type methods, diverges while the θ-MSUPG method gives a regular solution.

To study larger values of λ in the UCM case, we used a coarser mesh than $\mathcal{M}_1$ denoted by $\mathcal{M}_0$. For $\lambda = 0.125$ and mesh $\mathcal{M}_0$, all methods give a regular solution on the middle of the flow. On the meshes $\mathcal{M}_1$ and $\mathcal{M}_2$, the fixed point diverges with the SUPG type methods while the θ-MSUPG method gives a solution which stabilizes towards a weak solution (mesh $\mathcal{M}_2$: number of iterations : 50438, relative error between the last two iterations : $1.07e-006$). Thus, in the case of the UCM model, we have two types of approximate solutions. With mesh refinement, the weak solution would become more attractive for the θ-MSUPG method, while the fixed point diverges for the SUPG type methods. This kind of phenomenon is also observed in the case of the flow in a 4 : 1 contraction for the UCM model (*cf.* [13][14][15]) : the coarsest mesh gives

a regular solution, then, with mesh refinement, the fixed point applied to the methods using a SUPG type upwinding diverges (High Weissenberg Number Problem) while the θ-MSUPG method gives a solution that stabilizes around a weak type solution, which is characterized by the appearance of a slip at the downstream wall.

Thus, in the case of the UCM model, to give an element of explanation of the problem of the High Weissenberg number problem, we may conjecture that : first, in the case of a $4:1$ contraction, there would exist a weak solution (without excluding the possible existence of a joint strong solution, with a corner singularity), secondly, that this weak solution would become more attractive with mesh refinement and thirdly, that in this case, the iterative methods using a FEM of SUPG type diverge, while we obtain an eventual convergence of the θ-MSUPG methods towards the weak solution as in the case of the flow in a channel, as seen in this paragraph. In fact, the high Weissenberg number problem would perhaps occur for any Weissenberg number, as soon as we sufficiently refine the mesh at the downstream wall of the contraction (see [15], where we observe the divergence of the SUPG method for $We = 0.8$ and the appearance of a slip for $We = 0.6$).

3.3.4. Influence of the mesh, curves in norm of the energy of the iterates. To study the influence of the geometry of the mesh on the approximation of weak solutions with discontinuities and little regularity, the 2 triangles of the mesh $\mathcal{M}_1$ which have in common the vertex of coordinates $(2,1)$, as well as the two other pairs of triangles having each in common the vertices of coordinates $(4,1)$ and $(6,1)$, have been repositioned to obtain a uniform mesh along the boundary (see Fig. 14, upper left-hand graphs). The new mesh obtained is noted $\mathcal{M}_1'$ (see Fig. 14). The upper right-hand graph of Fig. 11 shows a cross-section of the solutions u_1 and σ_{11} obtained on the mesh $\mathcal{M}_1'$ (dashed lines), with a vanishing of the oscillations (see also Fig. 7 and Fig. 15). We have also tested the mesh $\mathcal{M}_2'$ obtained by successive refinements of the mesh $\mathcal{M}_1'$, this mesh is of the same size than the mesh $\mathcal{M}_2$ on Γ_w, but it is more regular (see Fig. 14, lower left-hand graphs).

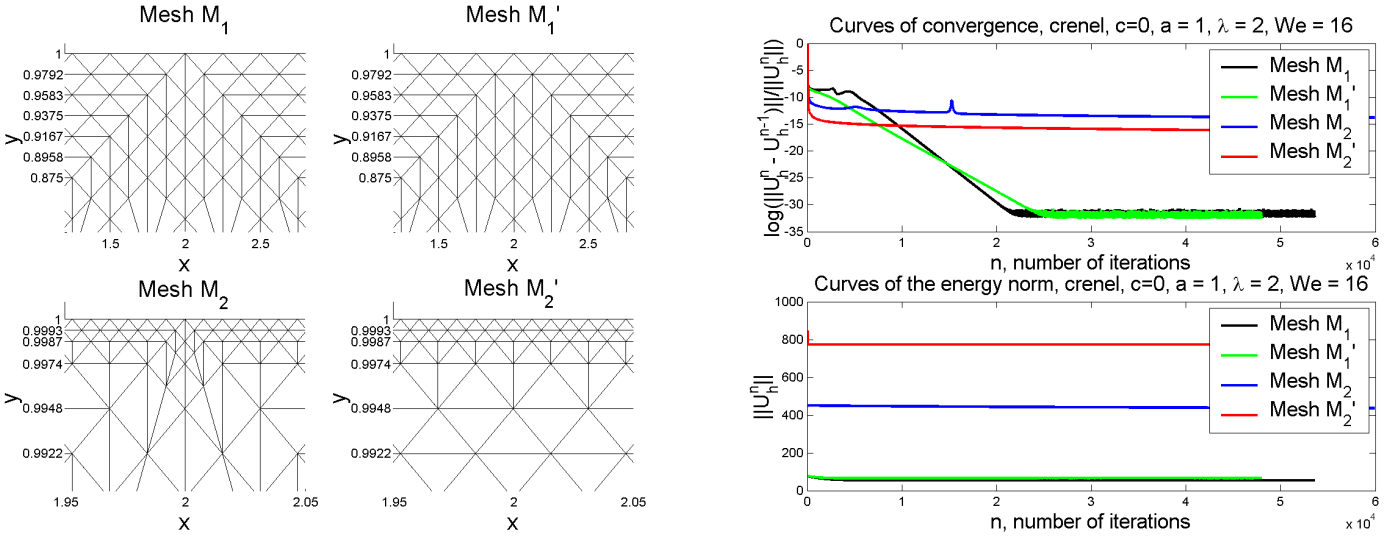

Fig. 14. Left graphs : meshes $\mathcal{M}_1$ and $\mathcal{M}_2$ and corresponding meshes $\mathcal{M}_1'$ (992 triangles, 529 vertices) and $\mathcal{M}_2'$ (9584 triangles, 5326 vertices). Right graphs : curves of convergence and curves of the energy norm of the successive iterates of the fixed point $(\mathcal{FP}) : n \to \|(\sigma_h^n, u_h^n, p_h^n)\|$. UCM model, boundary conditions on the component u_1 of the velocity of "crenel"-type, $a = 1$, $\lambda = 2$, $We = 16$, (DBC). Parameters : $(\theta, \delta, \mu, c) = (\frac{10}{11}, \frac{1}{10}, 2, 0)$. MSUPG term of upwinding : $\delta\lambda B(u_h^n, \tau)$. FE space : $P_1^4 \times P_2^2 \times P_1$-continuous. Results on the meshes $\mathcal{M}_1, \mathcal{M}_1', \mathcal{M}_2, \mathcal{M}_2'$.

Figure 15 represents a cross-sectional view of the solutions u_1 and σ_{11} obtained on the more regular meshes $\mathcal{M}_1'$ and $\mathcal{M}_2'$. The corresponding curves of convergence are those of Fig. 14 (with

$c = 0$), they are not completed, with however a quasi-constant norm of the energy of the last iterates. The use of regular meshes at the boundary Γ_w significantly improves the appearance of the approximate solutions in the neighbourhood of this one.

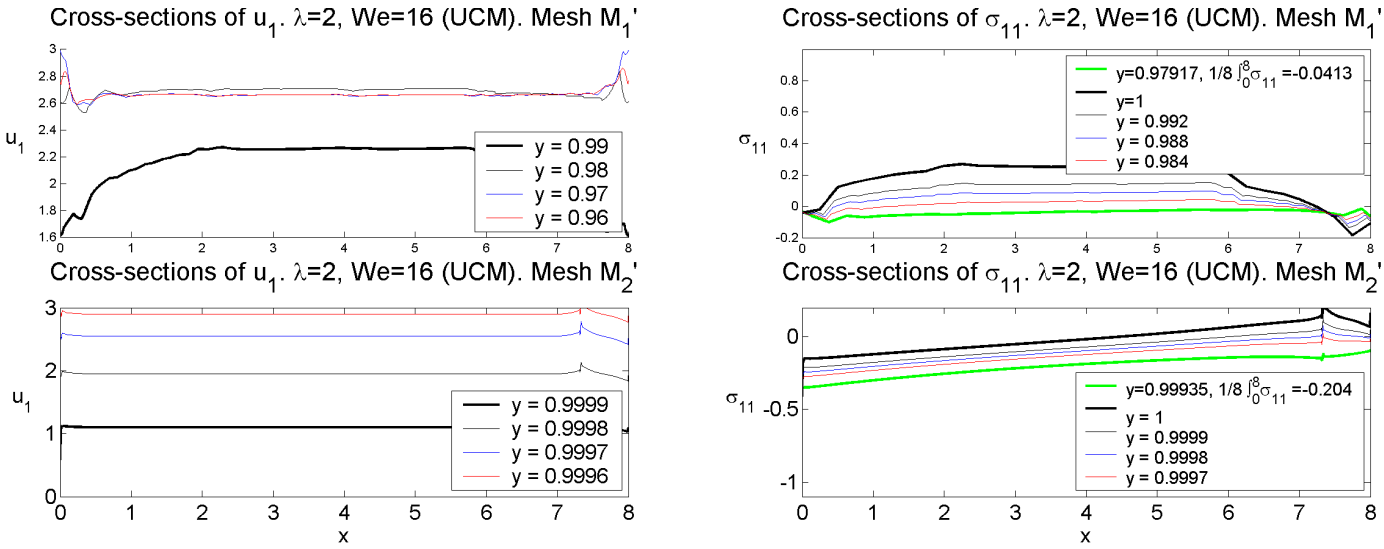

Fig. 15. Upper convected Maxwell model, §3.3, "Crenel". Figure corresponding to Fig. 11, with here, the results obtained on the meshes $\mathcal{M}_1'$ and $\mathcal{M}_2'$. Left graphs : cross-sections of u_1 along the lines $y = 0.96, 0.97, 0.98$ (thin line) and $y = 0.99$ (thick line) for the mesh $\mathcal{M}_1'$ and $y = 0.9996, 0.9997, 0.9998$ (thin line) and 0.9999 (thick line) for the mesh $\mathcal{M}_2'$. Right graphs : cross-sections of σ_{11} along the lines $y = 0.984, 0.988, 0.992$ (thin line) and $y = 1$ (thick line) for the mesh $\mathcal{M}_1'$ and $y = 0.9997, 0.9998, 0.9999$ (thin line) and $y = 1$ (thick line) on the mesh $\mathcal{M}_2'$. Cross-section of σ_{11} along the line $y = \beta$ with, on the mesh $\mathcal{M}_1'$: $\beta = \frac{47}{48} \sim 0.9792$, mean value $\frac{1}{8}\int_0^8 \sigma_{11}(x, \beta)\, dx = -0.0413$, on the mesh $\mathcal{M}_2$: $\beta = \frac{1535}{1536} \sim 0.9993$, mean value $\frac{1}{8}\int_0^8 \sigma_{11}(x, \beta)\, dx = -0.2044$.

3.4. Dirichtlet condition : Poiseuille regular flow imposed at the inflow and outflow. We consider the case of the upper convected Maxwell model, with boundary conditions of type (DBC). The extra-stress tensor is imposed at the inflow boundary and the velocity is imposed at the inflow and outflow boundary. The conditions at the boundary are given by the Poiseuille flow of class $\mathcal{C}^1(\Omega)$ given by Eqn. (3) : we set $u_0 = 4(1 - y^2)$ and σ_0 is given by the relation (7), with $u = 4(1 - y^2)$ in this one, *i.e.* :

$$\sigma_{011} = 2\lambda u_{01,2}^2, \ \sigma_{012} = u_{01,2}, \ \sigma_{022} = 0. \tag{7}$$

In a similar way to the previous §, we choose $p^f = 0$ on Ω_L. With this choice of boundary conditions, the continuous problem $(\mathcal{Q})$ admits as a solution the Poiseuille flow (σ, u, p) given by (3), (7) and this solution belongs to the FE space $P_2^4 \times P_2^2 \times P_1$-continuous. When solving the approximate problem $(\mathcal{Q}_h)$ with this FE space, with as the starting iteration in the fixed point scheme $(\mathcal{FP})$, the solution of the Stokes problem, then the fixed point converges in one iteration to (σ, u, p), up to round-off errors (see Fig. 16, lower left graph, the beginning of the curve of convergence). With rounding errors, when we continue the iterative process, then if λ is large enough, instabilities appear in the fixed point process. These instabilities depend on the mesh size, the coefficients c and μ of the fixed point method, the type of FE spaces and the choice of the upwinding. For example, for $\lambda = 0.6$ and the use of the θ-MSUPG method, we observe when solving the approximate problem $(\mathcal{Q}_h)$ on the mesh $\mathcal{M}_3$ (see Fig. 16, upper left-hand graph), a curve of the relative error between two successive iterations of the fixed point $(\mathcal{FP})$, which stabilizes with oscillations, around a plateau (see Fig. 16, lower left-hand graph).

On the other hand, we obtain velocity iterates that stabilize in the middle of the flow, towards the weak solution given by (4) (see Fig. 16, on the lower-right hand graph, the simulation result obtained for the P_2-continuous approximation of the tensors). For the SUPG method (with $c = 1000$ in $(\mathcal{FP})$) or the θ-SUPG method (with $c = 1$ in $(\mathcal{FP})$) and this value of $\lambda = 0.6$, the fixed point diverges, with the energy norm of the error between two successive iterations which tends to $+\infty$. We have not observed any wall slip for this type of decentering. The P_1-continuous approximation of the tensors gives similar results (see Fig. 16, upper right-hand graph, simulation result for the θ-MSUPG method).

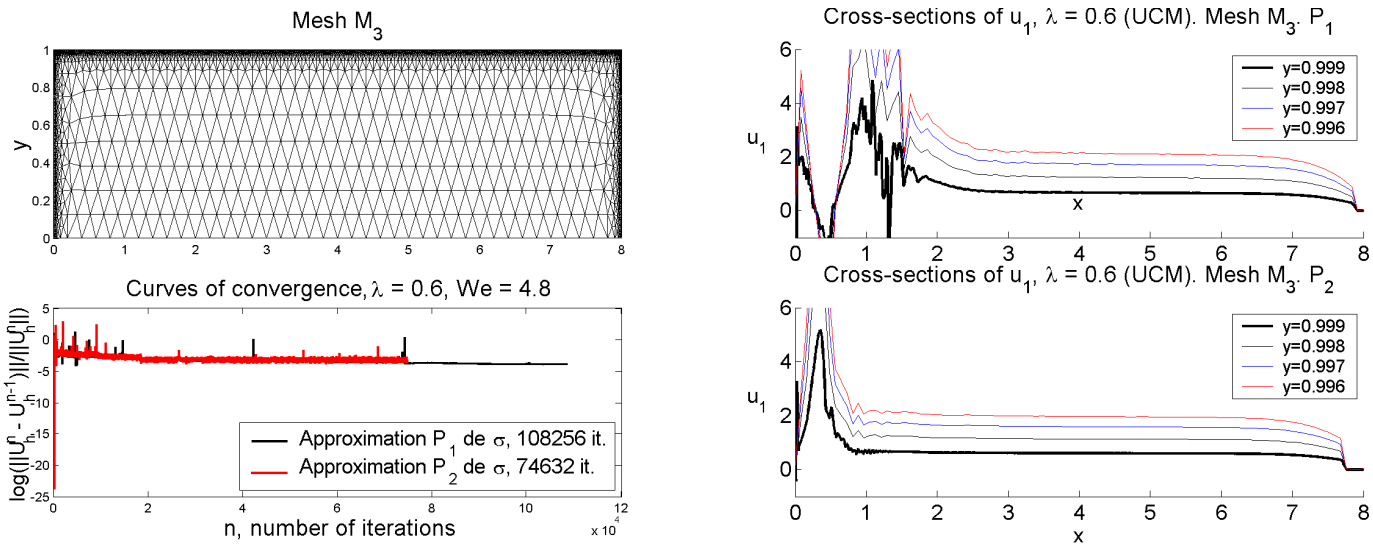

Fig. 16. Upper convected Maxwell model, Poiseuille regular flow imposed at the inflow and outflow boundary. Left graphs : Mesh $\mathcal{M}_3$ (6436 triangles, 3655 vertices, size h of the mesh of Γ_w : for $0.25 \leq x \leq 7.95, h = \frac{1}{80}$ and at the extremities, $h = \frac{1}{640}$) and curves of convergence. Right graphs : cross-sections of u_1 along the lines $y = 0.996, 0.997, 0.998$ (thin line) and $y = 0.999$ (thick line). UCM model, $a = 1$, $\lambda = 0.6$, $We = 4.8$, (DBC). Parameters : $(\theta, \delta, \mu, c) = (\frac{10}{11}, \frac{1}{10}, 2, 1)$. MSUPG term of upwinding : $\delta\lambda B(u_h^n, \tau)$. Approximation P_1 or P_2-continuous of the tensors. Results on the mesh $\mathcal{M}_3$. Number of unknowns for the approximation $P_1^4 \times P_2^2 \times P_1$-continuous : 42110 unknowns, for the approximation $P_2^4 \times P_2^2 \times P_1$-continuous : 72380 unknowns.

Thus, at the beginning of the process, the solution is reached exactly, up to round-off errors. Then, because of the round-off errors, the iterate of the fixed point moves away from the exact solution and either stabilizes towards a solution close to the weak solution, on the median part of the flow (without obtaining the convergence of the fixed point), or starts to diverge. Thus, in the latter case, everything happens as if the fixed point was repulsive, as already remarked by André Fortin in the case of a flow in a contraction.

We are thus in presence of two solutions of the continuous problem, when the Weissenberg number increases, the weak solution becomes attractive for the θ-MSUPG and the fixed point diverges for the SUPG or θ-SUPG method, in spite of the presence of a continuous solution

In the case of a flow through a 4 :1 contraction, with this type of boundary conditions and values of $We = 8\lambda$ close to 1 we obtain, with the θ-MSUPG method, the convergence of the fixed point iteration to a solution whose velocity shows a slip at the downstream wall of the flow (*cf.* [13][14][15]). For this kind of flow, when we refine the mesh along the downstream wall of the contraction, the fixed point becomes divergent when using SUPG or Lesaint-Raviart type methods (problem of the High Weissenberg Number). In the case of the θ-SUPG method, the fixed point remains convergent, with a rate of convergence which increases towards 1 when the size of the mesh of the downstream wall decreases. On the one hand, we observe

a mesh convergence of the solutions obtained on each mesh. On the other hand, we observe a convergence of these solutions, on a part of the downstream flow, towards a solution of the type of the weak solution of Proposition 1, Eqn. (4), with a downstream wall slip that can present more or less pronounced irregularities depending on the type of FE and meshes used (*cf.* [13][14][15]).

Fig. 17 describes cross-sectional views of the components σ_{11} and σ_{22} of the extra-stress tensor obtained on the mesh $\mathcal{M}_3$ with the θ-MSUPG method. On this figure, we notice that σ_{11} takes values close to the value $-\frac{1}{\lambda}$ on the first one third of the wall Γ_w, with the mean value $\frac{1}{3}\int_0^3 \sigma_{11}(x,1)\,dx = -1.3742$ in the case of the P_1 approximation and the mean value $\frac{1}{3}\int_0^3 \sigma_{11}(x,1)\,dx = -0.5226$ in the case of the P_2 approximation. This gives on this part of the wall, a value of C_σ relatively close to $-\frac{1}{\lambda} \sim -1.67$.

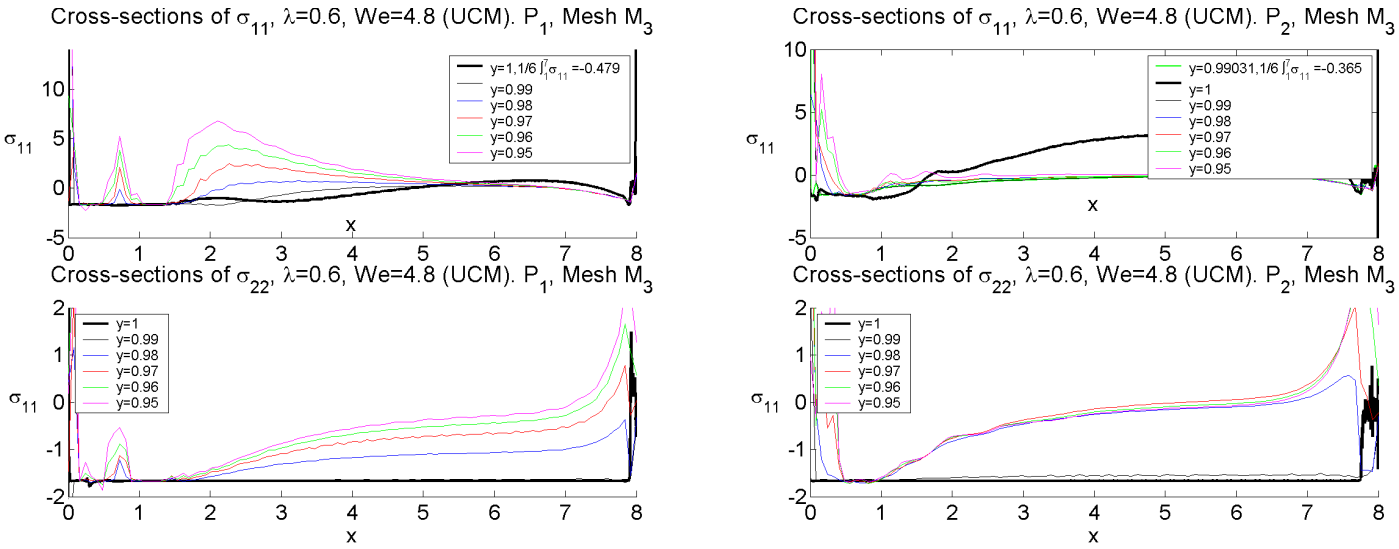

Fig. 17. Upper convected Maxwell model, §3.4, Poiseuille (continuation of Fig. 16). Left graphs : case of the P_1-continuous approximation of σ, cross-section of the components σ_{11} and σ_{22} of the extra-stress-tensor along the lines $y = 0.95, 0.96, 0.97, 0.98, 0.99$ (thin line) and $y = 1$ (thick line). Right graphs : case of the P_2-continuous approximation. On the upper graphs : cross-section of σ_{11} along the line $y = \beta$, with, for the approximation P_1, $\beta = 1$, $\frac{1}{6}\int_1^7 \sigma_{11}(x,\beta)\,dx = -0.4787$ and for the approximation P_2, $\beta = 0.9903$, $\frac{1}{6}\int_1^7 \sigma_{11}(x,\beta)\,dx = -0.3654$. $\frac{1}{\lambda} \sim 1.67$.

We notice in Table 4, within the framework of the θ-MSUPG method on the mesh $\mathcal{M}_3$, a stabilization, on a part of the domain, of the velocity and the components σ_{12} and σ_{22} of the extra-stress tensor towards the weak solution of Proposition 1 given by Eqn. (4). With the notations of §3.1 for the norms $\|\,.\,\|_A$ and $\|\,.\,\|_{F,F^\star}$, let $U^f = (\sigma^f, u^f, p^f)$ be the the weak solution, let U^i be the approximate solution obtained with the P_i approximation of the tensors, we have the ratios :

$$\frac{\|U^f - U^1\|_{F,F^\star}}{\|U^f - U^2\|_{F,F^\star}} = 1.25, \frac{\|U^f - U^1\|_A}{\|U^f - U^2\|_A} = 0.98,$$

which indicate a deviation from the weak solution on the restricted part of the domain of the same order for both types of approximation (P_1 or P_2-continuous approximation), with a better approximation of the weak solution u^f near the boundary, in the case of the P_2 approximation

of the tensors (see Tab. 4, and Fig. 16).

θ-MSUPG method , $(\theta,\delta,\mu,c)=(\frac{10}{11},\frac{1}{10},2,1)$, mesh $\mathcal{M}_3$, $a=1$, $\lambda=0.6$, $\frac{1}{\lambda}=1.67$, (DBC).						
Appr. P_1/P_2	$\frac{1}{6}\int_1^7 \sigma_{11}(x,1)\,dx$	$\frac{1}{6}\int_1^7 \sigma_{12}(x,1)\,dx$	$\frac{1}{6}\int_1^7 \sigma_{22}(x,1)\,dx$	$\frac{1}{6}\int_1^7 u_1(x,0.99)\,dx$	$\frac{1}{6}\int_1^7 u_2(x,0.99)\,dx$	$\frac{1}{6}\int_1^7 \tilde{p}(x,1)\,dx$
P_1 contin.	-0.4787	2.3628e-004	-1.6675	2.8752	-0.0099	-1.0922
P_2 contin.	1.8207	-0.0024	-1.6659	2.6701	-0.0006	-1.3110
L^1-norm	$\|\sigma_{11}-\sigma_{11}^f\|_F$	$\|\sigma_{12}-\sigma_{12}^f\|_F$	$\|\sigma_{22}-\sigma_{22}^f\|_F$	$\|u_1-u_1^f\|_{F^\star}$	$\|u_2-u_2^f\|_{F^\star}$	$\|\tilde{p}-p^f\|_F$
P_1 contin.	0.7752	0.0009	0.0010	0.6556	0.1935	0.8638
P_2 contin.	1.1920	0.0027	0.0012	0.0325	0.0069	0.7533
L^1-norm	$\|\sigma_{11}-\sigma_{11}^f\|_A$	$\|\sigma_{12}-\sigma_{12}^f\|_A$	$\|\sigma_{22}-\sigma_{22}^f\|_A$	$\|u_1-u_1^f\|_A$	$\|u_2-u_2^f\|_A$	$\|\tilde{p}-p^f\|_A$
P_1 contin	2.0489	0.3630	0.5679	0.0284	0.0100	0.9363
P_2 contin.	1.6845	0.3741	0.7578	0.1210	0.0754	1.0216

Table 4. Upper convected Maxwell model, §3.4, Poiseuille (continuation of Figs. 16-17). Convergence study. P_1 or P_2-continuous FE approximation of σ. The triple (σ,u,p) is the solution of the approximate problem $(\mathcal{Q}_h)$ and (σ^f,u^f,p^f) is the weak solution of the Proposition 1, Eqn. (4), with $U_0=\frac{8}{3}$. On the boundary Γ_w, $\sigma_{11}^f=C_\sigma$ is estimated by the mean value $\frac{1}{6}\int_1^7\sigma_{11}(x,1)\,dx$, on Ω_L, $C_p=0$. $\frac{1}{\lambda}=1.67$. Number of iterations : 108256 (P_1) and 74632 (P_2), relative error between the last two iterates : $2.13e-002$ (P_1) and $2.38e-002$ (P_2).

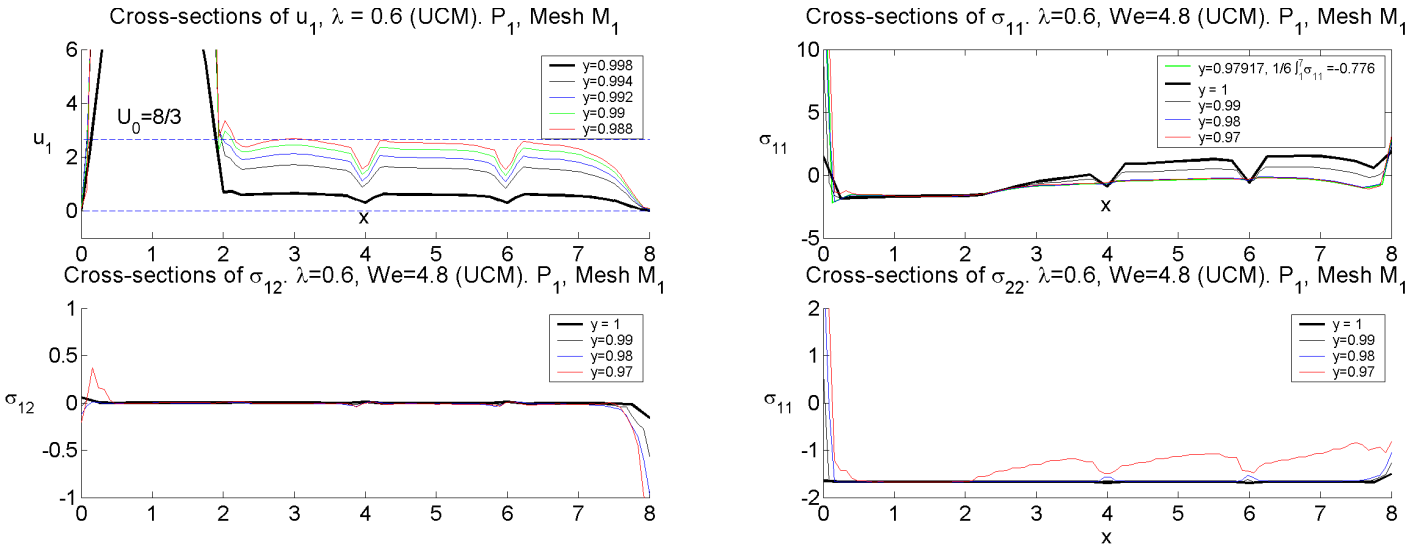

Fig. 18. Upper convected Maxwell model, §3.4, Poiseuille (continuation of Figs. 16-17). Approximation on the mesh $\mathcal{M}_1$. Cross-sections of u_1 along the lines $y=0.988,0.99,0.992,0.994$ (thin line) and $y=0.998$ (thick line) and cross-sections of the components of the extra-stress-tensor σ along the lines $y=0.97,0.98,0.99$ (thin line) and $y=1$ (thick line) as well as along $y=\beta=\frac{47}{48}\sim 0.9792$ for σ_{11}, $\frac{1}{6}\int_1^7\sigma_{11}(x,\beta)\,dx=-0.7757$. Parameters of $(\mathcal{FP})$: $(\theta,\delta,\mu,c)=(\frac{10}{11},\frac{1}{10},2,1)$. Number of iterations : 1178379, relative error between the last two iterates : $1.15e-006$.

We notice that the curves of convergence of Fig. 16 reach a plateau. The Figure 18 presents a result of simulation obtained on the mesh $\mathcal{M}_1$, with here an improvement of the convergence of the fixed point method (with a relative error between the last two iterates of $1.15e-006$). We obtain similar results with the mesh $\mathcal{M}_3$, with here, $\beta=\frac{47}{48}\sim 0.9792$, a mean value of $\bar{\sigma}_{11}=$

$\frac{1}{6}\int_1^7 \sigma_{11}(x,\beta)dx = -0.7757$ and the deviation from the mean in norm on F_β : $\frac{1}{6}\int_1^7 |\sigma_{11}(x,\beta) - \bar{\sigma}_{11}|\,dx = 0.4505$. On the boundary, σ_{11} takes the mean value of $\frac{1}{2}\int_{0.3}^{2.3} \sigma_{11}(x,1)dx = -1.6787 \pm 0.0543$, close to $-\frac{1}{\lambda}$, before growing, in mean, from $y \geq 2.3$.

4. Conclusion. In the case of a flow through a channel, on a given mesh, the solutions of class $\mathcal{C}^1$ of Proposition 1, when they exist, appear stable for small values of λ. This stability can be understood in the sense that, when the fixed point $(\mathcal{FP})$ converges, the approximate solution of the problem $(\mathcal{Q})$, with various boundary conditions, stabilizes to these solutions on a part of the flow or converges to one of these solutions, as in the case of the choice of boundary conditions given by the regular Poiseuille flow as in §3.4. When λ increases or when the existence of the solution of class $\mathcal{C}^1$ is lost as in the case of the COM model, they are the weak solutions of Proposition 1, which then appear stable. As in the case of §3.3.3, in the UCM case, these solutions can also become stable with the mesh refinement. In §3.3.3, for the COM model with $\lambda \leq \lambda_c$, the approximated solution stabilizes well, with the mesh refinement, towards a regular solution in the case of the θ-MSUPG method. This stabilization occurs also, more slowly, during the fixed point process, for a SUPG type decentering. The θ-SUPG method gives an intermediate approximate solution between the weak solution and a regular solution.

In the case of the UCM model, the stabilization of the approximated solution towards a weak solution depends on the FE methods used : methods SUPG, θ-SUPG or θ-MSUPG. Thus, the fixed point method coupled to a FEM of type θ-SUPG, after converging for small values of λ to a regular solution (for example to the Poiseuille flow of class $\mathcal{C}^1(\Omega)$, if this one is a solution of the problem $(\mathcal{Q})$, as in §3.4) starts to diverge when λ increases. With a FEM of type θ-MSUPG, the fixed point method continues to converge, more or less well (for bounded λ values) and gives a solution which stabilizes towards a weak solution on a part of the flow or, as in §3.3, which converges with the mesh refinement to a weak solution. This shows a role of the weak solutions in the framework of the FEM approximation of the problem $(\mathcal{Q})$. In the case of the UCM model, this role only appears with the use of the θ-MSUPG type methods, with the appearance of these solutions, as well as, eventually, by the divergence of the fixed point methods using a SUPG type decentering in the variational formulation.

There is an infinite number of weak solutions defined up to the constant C_σ, which is the value taken on the boundary Γ_w by the weak solution σ_{11}^f. In the simulations, this value appears relatively constant on Γ_w and could be given by $C_\sigma = -\frac{1}{\lambda}$ in the sense of the limit given by a relation of the type (8) ou (8'). It could also depend on the boundary conditions as well as on the size of the mesh at the wall.

It should be noted that the preponderant role played here by the term $\sigma\omega(u) - \omega(u)\sigma - a(d(u)\sigma + \sigma d(u))$ in the existence of weak solutions and their approximation, underlines the interest of studying viscoelastic models obtained by neglecting the transport term $u.\nabla\sigma$, as for example in [10].

In the case of a flow through a 4 :1 contraction, when using a θ-MSUPG method, we observe the appearance of solutions whose velocity shows a slip at the downstream wall of the flow (*cf.* [12], [13], [14], [15]), these one are similar to the weak solutions of Proposition 1. This suggests the existence of weak solutions for this type of flow. The phenomenon of the high Weissenberg number occurs when the fixed point starts to diverge with the mesh refinement, for relatively high numbers of We. For the SUPG methods, on the meshes that precede the divergence phenomenon, the peak of σ_{11} at the singularity of the reentrant corner of the contraction grows rapidly with the successive mesh refinements (*cf.* [15]). This phenomenon of the high Weissenberg number could then be explained in part by the existence of a weak solution and a joint solution of class $C^1(\Omega)$, whose existence remains an open problem, and by the difficulty of approximating these two kinds of solutions. The weak solution could be downstream of the flow of the type of the weak solution of Proposition 1 and the solution of class $C^1(\Omega)$

could have a corner singularity or a singularity along the downstream wall of the flow. With the mesh refinement, it would be the weak solution that would become the most stable, the numerical scheme would not be able to capture either the weak solution or the $C^1(\Omega)$ class solution and starts to diverge, which would produce the phenomenon. The θ-MSUPG method would capture the weak solution, with the problem of approximating a possible solution of class $C^1(\Omega)$ remaining open. It is to be noted that in the case of the COM model, we can envisage that the problem does not admit any solution of class $C^1(\Omega)$ from a critical Weissenberg number, but that it keeps a weak solution.

References.

[1] Alfonso A., Alves M., Pinho, F., Oliviera P. : Application of the log-conformation tensor approach to three dimensional viscoelastic flows. CMNE/CILAMCE 2007 Porto, 13 a 15 de Junho, 2007.

[2] Fattal, R., Kupferman, R. : Constitutive laws for the matrix-logarithm of the conformation tensor J. Non-Newtonian Fluid Mech., 123 (23), (2004) pp. 281-285.

[3] Fortin, M., Fortin, A. : A new approach for the FEM simulation of viscoelastic flows, J. Non-Newtonian Fluid Mech., 32 (1989), 295-310.

[4] Fortin, A., Guénette, R., Pierre, R. : On the discrete EVSS method. Comput. Methods Appl. Mech. Engrg. 189 (2000), n° 1, 121-139.

[5] Fortin, M., Pierre, R. : On the convergence of the mixed method of Crochet and Marchal for viscoelastic flows, Comp. Methods Appl. Mech. Engrg., 73 (1989), 341-350.

[6] Guillopé, C., Saut, J-C. : Global existence and one-dimensional non linear stability of shearing motions of viscoelastic fluids of Oldroyd type, Modél. Math. Anal. Numér., **24**, n° 3 (1990), 369-401.

[7] Hinch E.J. : The flow of an Oldroyd fluid around a sharp corner J. Non-Newtonian Fluid Mech., 50 (1993), pp. 161-171.

[8] Keunings, P. : In : Tucker Ch. III (ed.) Computer Modeling for Polymer Processing, pp. 403-469. Munich : Hanser Verlag, 1989.

[9] Marchal J.M., Crochet, M.J. : A new finite element for calculating viscoelastic flow, J. Non-Newtonian Fluid Mech., 26 (1987), pp. 77-114.

[10] Picasso, M., Rappaz, J. : Existence, a priori and a posteriori error estimates for a nonlinear three-field problem arising from Oldroyd-B viscoelastic flows, Mathematical Modelling and Numerical Analysis-Modélisation Mathématique et Analyse Numérique, 35 (2001) n° 5, 879-897.

[11] Ruas, V. : An optimal three-field finite element approximation of the Stokes system with continuous extra stresses, Japan Journal of Industrial and Applied Mathematics, 11, (1994), 113-130.

[12] Sandri, D. : On a FEM method for a linearized version of the Oldroyd Problem, Comput. Methods Appl. Mech. Engrg, 191 (2002), pp. 5045-5065.

[13] Sandri, D. : Numerical study around the corotational Maxwell model for the viscoelastic fluid flows. Eur. J. Mech. B Fluids, 24, (2005), n° 6, 733-750.

[14] Sandri, D. : Finite element method for viscoelastic fluids flows : approximation of the upper convected Maxwell model and study of a wall slip. Publication de l'Institut Camille Jordan n° 408, 33 p. (2018).

[15] Sandri, D. : Finite element method for viscoelastic fluids flows : approximation of the upper convected Maxwell model and study of a wall slip. Study of convergence mesh. Publication de l'Institut Camille Jordan n° 411, 30 p. (2021).

[16] Trebotich, D. : Toward a solution to the high Weissenberg number problem PAMM. Proc. Appl. Math. Mech. 7, 21000732100074 (2007).